Evolving Shallow-conduit Container Affects the Lava Fountaining during the 2021 Fagradalsfjall Eruption, Iceland

Eva P. S. Eibl (eva.eibl@uni-potsdam.de)
University of Potsdam https://orcid.org/0000-0002-0667-0035

Thor Thordarson
University of Iceland

Ármann Höskuldsson
University of Iceland

Egill Á. Gudnason
ISOR, Iceland GeoSurvey

Thoralf Dietrich
University of Potsdam

Gylfi Páll Hersir
formerly: ISOR, Iceland GeoSurvey

Thorbjörg Ágústsdóttir
ISOR, Iceland GeoSurvey

Research Article

Keywords:

Posted Date: March 16th, 2022

DOI: https://doi.org/10.21203/rs.3.rs-1453738/v1

Evolving Shallow-conduit Container Affects the Lava Fountaining during the 2021 Fagradalsfjall Eruption, Iceland

Eva P. S. Eibl[a]*, Thor Thordarson[b], Ármann Höskuldsson[b], Egill Á. Gudnason[c], Thoralf Dietrich[a], Gylfi Páll Hersir[c,d], Thorbjörg Ágústsdóttir[c]

a: University of Potsdam, Institute for Geosciences, Karl-Liebknecht-Str. 24/25, Potsdam-Golm
*: eva.eibl@uni-potsdam.de
b: University of Iceland, Sturlugata, Reykjavik, Iceland
c: ISOR, Iceland GeoSurvey, Urdarhvarf 8, Reykjavik, Iceland
d: Reykjavik, Iceland, gylfi.pall@outlook.com

Keywords: seismology, volcanic tremor, crater collapses, magma viscosity, lava fountaining, vent evolution

1 Main Findings

- Our seismometer recorded 7058 lava fountain episodes of the Fagradalsfjall eruption, Iceland, between 2 May and 14 June 2021.
- We define six periods with distinct fountaining patterns featuring fast changing pulse duration, stable pulse duration and coexisting short and long pulses.
- The pattern is affected by processes such as an evolving shallow-conduit container from 2 to 11 May, crater rim collapses, accumulating degassed magma and the vent dimensions.

2 Abstract

Pulsating behaviour is observed in volcanic phenomena ranging from caldera collapses to explosions, spattering or lava fountaining. The repeating processes can define irregular, regular or systematically changing patterns. These patterns yield information about the subsurface structure, which often is not considered in detail. We analyse the pattern of 7058 lava fountaining episodes that occur between 2 May and 14 June 2021 during the Fagradalsfjall eruption, Iceland. Our seismometer records the lava fountaining episodes as tremor pulses. We analyse the seismic tremor amplitude, the pulse duration, the repose time and the sum of pulse duration and repose time (cycle duration). We define six periods characterised by different patterns: Three periods feature long pulses that exponentially shorten with time. One period features coexisting long and short pulses in a haphazard sequence. One period shows a stable pulsing duration but increasing repose time and one period has stable, short pulses and repose times. We conclude that the episodic fountaining starts because a shallow-conduit container forms on 2 May shifting the magma degassing from sustained continuous to an episodic state. This situation evolves until 11 May when a semi-stable state is reached. The length of the repose times are most likely influenced by the amount of outgassed magma present in the uppermost part of the shallow conduit. Finally, we suggest that the vent is mechanically eroded and widens with time causing increasing seismic tremor amplitudes. However, the trends are frequently punctuated by partial crater wall collapses that temporarily disrupt the system.

3 Introduction

Tremor is an emergent, long-lasting volcano-seismic signal that precedes and accompanies eruptions (Zobin, 2017). It can serve to distinguish sources and eruptive activity styles (Falsaperla et al., 2005; Langer et al., 2009) for example when the eruption location is obscured by poor visibility. While tremor can persist for years (Cannata et al., 2008; Swanson et al., 1979) it can also transition to a start and stop behaviour (Eibl et al., 2017b) or appear episodically (Andronico et al., 2021; Heliker and Mattox, 2003; Patrick et al., 2011; Privitera et al., 2003; Thompson et al., 2002; Zobin, 2013).

Pulsating behaviour occurs in different volcanic contexts ranging from caldera collapses to explosions, spattering or lava fountaining. Caldera collapses are often composed of several collapse events recorded as tremor pulses (Michon et al., 2007), repeating volcano-tectonic earthquakes (Gudmundsson et al., 2016; Tepp et al., 2020) or VLP earthquakes (Kumagai et al., 2001). For example, pulsatory eruptions are typified by a series of explosions (Dominguez et al., 2016). Fast repeating explosion patterns are also detected near erupting geysers (Azzalini and Bowman, 1990; Eibl et al., 2020; Munoz-Saez et al., 2015) where steam bubbles reach the surface and expel boiling water into the air. A perched lava channel can exhibit a cyclic pattern of lava level rise and spattering (Patrick et al., 2011). Finally, a sharp tremor increase has been observed to accompany lava fountaining at volcanoes worldwide (Alparone et al., 2003; Falsaperla et al., 2005; Heliker and Mattox, 2003; La Spina et al., 2015; McNutt, 1987; Privitera et al., 2003; Tanguy and Patane, 1984, e.g.).

Independent of these different contexts, tremor pulsing can occur in regular, irregular or systematically changing intervals. Stable repose times around 24 h with rare fluctuations up to 120 h and down to 8.4 h were reported at Pu'u 'Ō'ō from 1983 to 1986 (Heliker and Mattox, 2003). Privitera et al. (2003) reported regular lava fountaining on Etna in 1989 and successfully posteriori forecasted some eruptions using simple statistical methods. Based on 73466 eruptions Eibl et al. (2020) concluded that Strokkur geyser in south Iceland erupts on average every 3.7±0.9 min. Thompson et al. (2002) reported 23 to 48 explosions in each 3 min long time window recorded as tremor pulses during the 1999 eruption of Shishaldin Volcano, Alaska. These regular time-spaced pulses later transitioned to more irregular repose times where shorter and longer pauses coexisted.

Other examples with irregular repeat times have been recorded from eruptions on Hawaii and Etna. Pauses in the eruptive activity from 1989 to 2000 at Pu'u O'o (Kilauea volcano, Hawaii) were neither regular in duration nor in temporal spacing (Heliker and Mattox, 2003). The frequency of 64 lava fountains in 2000 was neither repeating at regular intervals nor showed a systematic change (Alparone et al., 2003). In 2011, nine lava fountain episodes took place in irregular 5 to 10 day long intervals (Carbone et al., 2015). In 2007, a perched lava channel within the Pu'u O'o flow field showed regular spattering every 40 to 100 min. Patrick et al. (2011) report two periods with fewer spattering events per day without commenting on likely reasons for the changes in duration of the events.

Systematic changes in repose time have been reported more rarely in association with lava fountaining events on Etna (Moschella et al., 2018; Spampinato et al., 2015). Another example are tremor pulses due to rock column collapses during caldera formation, as happened in 2007 at Piton de la Fournaise. They became more closely spaced with time (Michon et al., 2007). The spacing pattern was in these cases unfortunately not investigated further.

Dominguez et al. (2016) developed an empirical relationship between median repose time and magma viscosity, based on eruptions at different volcanoes. However, whether changes in the magma viscosity systematically change the pulsing behaviour of one eruption remains an open question.

While regular, irregular or systematic changes within a pattern can take place, irregular patterns or systematic changes have not been investigated previously in detail. Triggers for these changes hence remain obscure. Here we investigate triggers that change the repeating tremor pattern of 7058 lava fountaining episodes that occurred in the Fagradalsfjall eruption on the Reykjanes Peninsula from 2 May to 14 June 2021.

The Reykjanes Peninsula, in Southwest-Iceland, links the Western Volcanic Zone and the South Iceland Seismic Zone of Iceland to the offshore Reykjanes Ridge. The Reykjanes Peninsula features several northeast trending volcano-tectonic lineaments, also referred to as volcanic systems (e.g., Clifton and Kattenhorn (2006); Jakobsson et al. (2008, 1978); Sæmundsson and Sigurgeirsson (2013); Sæmundsson et al. (2020); Thordarson and Höskuldsson (2008)). They are from east to west : (i) Brennisteinsfjöll, (ii) Krýsuvík, (iii) Fagradalsfjall, (iv) Svartsengi and (v) Reykjanes. These volcano-tectonic lineaments are highly oblique to the plate boundary and plate movement (Jakobsson et al., 1978; Sæmundsson et al., 2020). All volcano-tectonic lineaments except Fagradalsfjall host a high-temperature geothermal system.

In the last 3.5 ka the volcanic activity pattern was periodic, where 400 to 500 year-long eruption periods are separated by 800 to 1000 year-long periods of volcanic quiescence (Sæmundsson et al., 2020). Within each eruption period only one volcanic system is active at any one time. The activity appears to migrate from the east to the west at a temporal spacing of 100 to 200 years (Sæmundsson et al., 2020). The last eruption period ended in 1240 CE (Jonsson, 1983; Sæmundsson et al., 2020; Sigurgeirsson, 1995). The Fagradalsfjall lineament features both Weichselian subglacial volcanic edifices and Holocene lava flow fields. However, before 2021 it had not erupted in more than 6000 years (Sæmundsson and Sigurgeirsson, 2013) and hence does not follow this episodic pattern of volcanism on the Peninsula. The 2021 eruption at Fagradalsfjall may be signalling the onset of a new eruption period on the Reykjanes Peninsula (Çubuk-Sabuncu et al., 2021; Flóvenz et al., 2022; Geirsson et al., 2021).

We study the tremor during episodes of lava fountaining and outflow of the 2021 Fagradalsfjall eruption (section 4) applying a STA/LTA filter to data from a nearby seismometer (section 5). We consider the growth of Vent-5 (section 6.1) and the temporal tremor properties from March to mid June (section 6.2). We find systematic changes in the pulse duration with time (section 6.3), define different correlations behaviours of the pulse duration and repose time (section 6.4) and analyse the time window featuring both short and long pulses (section 6.5). We discuss the details of one pulse (section 7.1), reasons for the onset of the episodic fountaining (section 7.2), the decreasing and stable pulse duration (section 7.3), the gradual increase in the repose time (section 7.4), the coexistence of short and long pulses (section 7.5) and the linearly increasing seismic amplitude (section 7.6). We conclude that the fountaining pattern is affected by processes changing the boundary conditions and describe the evolving shallow-conduit container.

4 Background and Chronology of the Fagradalsfjall Eruption

After 781 years of quiescence (Jonsson, 1983; Sæmundsson et al., 2020; Sigurgeirsson, 1995), eruptive activity resumed on the Reykjanes Peninsula at approximately 20:30 UTC on 19 March 2021 (Icelandic Meteorological Office, 2021). The eruption at Geldingadalir within the Mt. Fagradalsfjall complex was preceded by 3 weeks of seismic unrest in the Fagradalsfjall region (Fischer et al., 2022; Sigmundsson et al., 2021). From 24 February it was associated with the emplacement of a 9 km long regional dyke between Fagradalsfjall and Keilir (Jonsdottir et al., 2021) (Fig. 1a).

On 19 March 2021 the eruption in Geldingadalir features 12 small vents each sitting on a 10 to 20 m long northnortheast-trending en-echelon fracture, briefly defining a 180 m long vent system. This initial activity becomes more and more localised and by 3:30 am (local time) on 20 March there are 8 vents. By daybreak it is confined to the two features that were later called Vents-1a and 1b. These are the only vents active until 5 April 2021 (Fig. 1b and c) and supply the majority of the lava initially emplaced in Geldingadalir. The magma effusion is characterised by steady bubble-bursting to weakly fountaining activity accompanied by continuous lava outflow.

At 12:00 on 5 April a new vent (2) opens about 800 m northeast of the original vents in Geldingadalir (Fig. 1b). The activity on Vent-2 begins in the same manner as for Vent-1. This is followed by series of new vent openings between Vent-1 and 2, with the last two (5 and 6) opening at 8:37 and 8:50 on 13 April (Fig. 1b and d). Vents 1a and 1b were the only still active vents on 29 and possibly 30 April. We refer to the vent opening and closing period from 19 March to 1 May 2021 as Stage 1.

Stage 2 is characterised by effusion through Vent-5 and lasts from 2 May to 11 September 2021. From April to 18 September, Vent-5 is the centre of activity. Vent-5 delivers lava to the flow field via internal (sealed) pathways along with episodic lava fountaining of variable intensity and periodicity (Fig. 1e to f and 2).

The final Stage 3 lasts from 12 to 19 September 2021 with one new lava outlet near the wall of Crater-5. This outlet is north of the former Vent-5. By the end of September 2021, the eruption has formed a volcanic cone rising about 120 m above the pre-eruption surface (Pedersen et al., 2022). The time-averaged magma discharge is steady at about

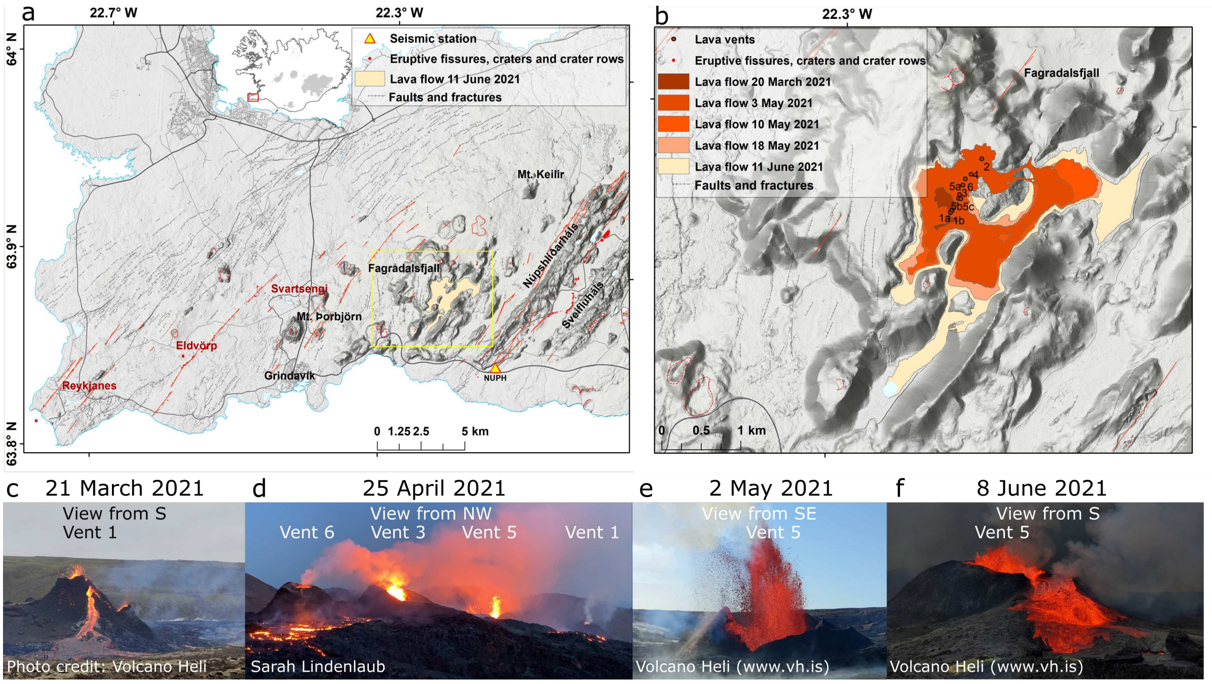

Figure 1: Overview of the eruptive site and instrument location. (a) Overview and location of the Reykjanes Peninsula, Iceland. The lava flow field (beige) and seismometer (triangle) are indicated. (b) Extent of the growing lava flow field and vent locations as derived in a collaboration of the National Land Survey of Iceland, the University of Iceland and the Icelandic Institute of Natural History. (c-f) Photos visualising the transition from steady lava outflow from Vent-1 (c, 21 March), to steady lava outflow from multiple vents (d, 25 April, Vent-2 and 4 not visible on photo), to lava fountaining (e, 2 May), to vigorous, splashing overflow at Vent-5 (f, 8 June).

$7{\pm}2.5\,m^3/s$ (DRE, range, 2 to $10\,m^3/s$, Landmaelingar Islands (2021); University of Iceland (2021). The total lava field covers about $5\,km^2$ and has an approximate DRE rock volume of $0.1\,\mathrm{km}^3$ (Bindeman et al., 2022).

5 Data Acquisition and Data Analysis

5.1 Instrument Setup

We installed a Trillium Compact 120 s seismometer (Nanometrics) as station NUPH (RR seismic network) at the southeast corner of Núpshlídarháls 5.5 km southeast of the eruptive site in Geldingadalir, Iceland (Fig. 1a). The instrument stood on a concrete base slab shielded from wind and rain using a bucket partly covered by rocks. The instrument was powered using batteries from 16 March, solar panels from 24 March and a wind generator at 10 m distance from 6 April 2021. Data were sampled at 200 Hz, they were stored on a Datacube and regularly downloaded. We used a compass to align the instrument to geographic north.

Wind speeds higher than 5 m/s create strong noise on our sensor above 1 Hz. Despite this noise, the data quality is good enough to detect volcano-seismic signals such as tremor.

5.2 Seismic Preprocessing

The seismic data are detrended, instrument response corrected to velocity, tapered and filtered between 1 and 4 Hz. We use the Pyrocko trace-viewer Snuffler to mark the start and end of the tremor pulses (Heimann et al., 2017). First, we use the built-in STA/LTA triggering algorithm (Trnkoczy, 2012) on the sum of the 3 component seismic recordings of station NUPH. We use STA windows of 60 to 120 s and three times larger LTA windows in a moving time window. STA/LTA markers are then moved to the pulse start and end. Finally, we manually review all markers and add, remove and time-correct them if necessary. We process the time window from 1 May to 14 June leading to 14116 markers (Eibl et al., 2022).

We define the **tremor pulse cycle duration** from the start of one pulse to the start of the next pulse (Fig 4e). The **tremor pulse duration** is defined from the start to the end of one pulse. The **tremor repose time** is defined from the end of one pulse to the start of the next pulse. Hence, the pulse duration plus repose time equals the pulse cycle duration.

We calculate root mean square (RMS) seismic ground velocity in 30 s long time windows and 50% overlap for the whole time period. We also calculate the mean RMS during a tremor pulse and in the repose time.

5.3 Video Camera Analysis for Kymograph

We analyse data from a camera by mbl.is (Morgunbladid) using a kymograph. This is an illustrative way of photo sequence analysis at geysers and volcanoes (Munoz-Saez et al., 2015; Witt and Walter, 2017). To create a kymograph we choose a vertical line from the ground through the active vent in all images, and plot the pixels' colour values of this line along a time axis. Video images are extracted at 1 frame per second. Using this time-space-plot we identify the lava fountain occurrence, height and duration as recorded by the camera.

6 Results

6.1 Eruption Behaviour and Growth of the Crater-5 Edifice

In the first 4 days, Vent-5 is surrounded by a few m-high ramparts which we call Crater-5 (Fig. 2a). Within two weeks, the crater grows quickly in height and dominates the other craters with a height of about 40 m on 30 April. A period of particularly rapid crater-wall growth at Vent-5 occurs between 10 and 17 May, when the wall height increases by 15 m. The total height is about 60 m in mid June. The walls of Crater-5 appear unstable until mid May but become more stable as they thicken with time and the surrounding lava flow field stabilizes the crater (Landmaelingar Islands, 2021). Overflow dominates in the south and northeast and thus these sides of the crater become less steep throughout May. From 30 April to 18 May the growing Crater-5 features frequent collapses from the walls on the western, eastern and northern side (Fig. 2a and Fig. 4f). From 15:45 on 30 April, cracks form in the Crater-5 walls resulting in a major outwards collapse of the southwestern flank towards the southwest (Fig. 2a and S1). This sliding was slow and persistent until 10:00 on 2 May. In the following days of May, several partial collapses occur daily. From 10 May and onwards about one daily collapse happens from the crater rim. After 18 May the only major collapse occurs at 4:18 on 10 June, when a circular fault forms along the crater rim and the inner part of the wall collapses into the crater. The collapse-related processes steadily widen the crater with time.

Through April Vent-5 is typified by a sustained and semi-steady activity of vesiculation (i.e., degassing), bubbling (i.e., outgassing), and intensifying fountaining, and lava out-

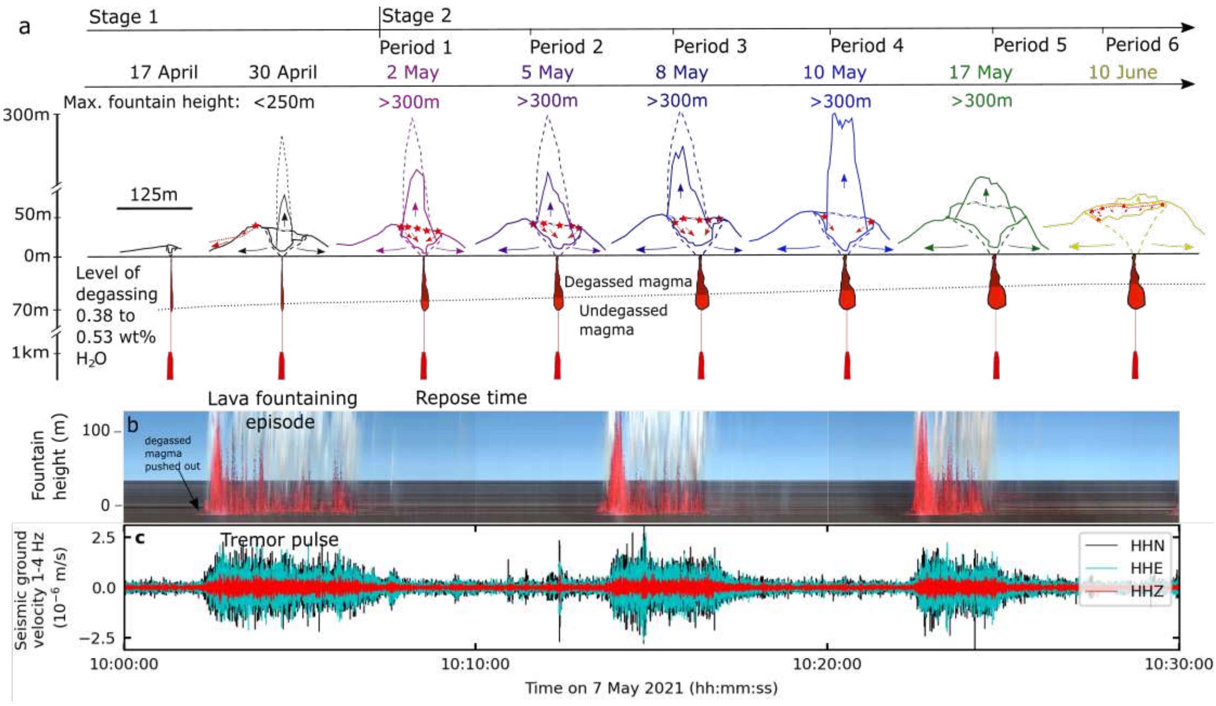

Figure 2: Growth, fountaining and collapses of Crater-5 from 17 April to 10 June. (a) Colored lines mark the crater shape at 14:00 on the respective date according to Payne (2021) and an exemplary (solid) and maximum (dashed) fountain height. Colored arrows show lava outflow into the fountain or the lava flow field. Red stars mark collapses in the crater while dotted red lines show the fault plane and red arrows the collapse direction. The red and dark red color indicates undegassed and degassed magma, respectively, accumulating in a shallow-conduit container evolving from 2 to 11 May. The red dike at 1 km depth feeds the eruption. The black dotted line indicates the depth at which degassing starts. (b) Kymograph of fountain height and (c) seismic ground velocity of 3 seismometer components.

flow. For example, the fountain height reaches 250 m by 30 April, compared to heights of only a few meters in the early stages (13 to 15 April) of Vent-5 activity. This pattern of Vent-5 activity is driven by the gradual evolution of the top 1 km of the plumbing system. The effusion of magma semi-steadily becomes focused on the shallow conduit of Vent-5, which culminates on 30 April when visible activity at Vents 1a and 1b stops. In the early hours of 2 May the pattern of activity described above was abruptly replaced by distinctly periodic activity, featuring episodes of lava outpouring, outgassing and fountaining each punctuated by distinct lulls in activity.

An episode normally begins with a vesiculation-/degassing-driven, and escalating rise of the free magma surface in the crater. Shortly after the onset of the lava outpouring, visible bubbling (i.e., outgassing) at the free magma surface intensifies rapidly and leads to bursting of fast rising and expanding mega-bubbles (tens of meters in diameter), peaking in a run-a-way outgassing driving the vigorous and high fountains that typify the early stages of each episode in the period from 2 to 18 May when the maximum fountain heights exceed 300 m. When maximum fountain height is reached, outgassing had outpaced degassing and for the reminder of the episode the activity becomes more pulsating. The fountaining vigor, intensity and height reduces in a semi-steady manner until the free magma surface drops abruptly and the episode comes to a sudden halt. At this stage, the bubble framework collapsed and outgassed lava residing in the crater retreats into the underlying shallow conduit compartment in a few minutes, leaving the crater empty during the repose time. From 18 May and onwards, the vigor of the activity in each episode was reduced significantly. The maximum fountain heights were much lower and the eruption behavior transitioned to a fast-moving, vigorous, splashing lava over-flowing the crater rims in conjunction with effective outgassing and weak fountaining.

6.2 Seismic Spectral Properties of the Effusive Tremor

The volcanic tremor starts at 20:45 UTC on 19 March 2021. From March to 1 May the eruptive tremor is continuous and characterised by energy below 3 Hz, strongest on the horizontal components (Fig. 3). The opening of new vents does not increase the tremor amplitude or spectral content recorded at NUPH. From 2 May the tremor energy increases in all frequency bands, it broadens to 6 Hz and frequencies around 4 Hz increase in strength (Fig. 3a and f and Fig. S2). By 10 June the tremor pulse peak amplitude has linearly increased threefold (Fig. 3a to e and 4a). At 5:00 UTC on 10 June this trend is disrupted when the tremor amplitude and energy in the spectrogram suddenly decrease (Fig. 3f and m).

Besides the long-term changes in the amplitude and frequency content of the tremor, the volcano enters a start and stop phase with episodic lava effusion from 2 May to 14 June. We record a tremor pulse during lava fountaining or vigorous outflow (Fig. 2b and c) and no outflow as no tremor. From 14 to 25 June continuous tremor and weak pulses reappear.

6.3 Gradual Temporal Changes in the Fountaining Duration and Repose Time

From 2 May to 14 June 2021, 7058 tremor pulses are recorded (Fig. 4). Pulses are detected on all three components of the seismometer (Fig. 4a). The tremor amplitude is similar on the north and east component throughout the time period (Fig. 4b). The seismic amplitude of the horizontal components is two times larger than the amplitude of the vertical component in the times of repose, and 3 to 4 times larger during pulses (Fig. 4b). The RMS amplitude of the tremor pulses increases linearly with time (Fig. 4a). It is, however, affected by wind noise for example from 25 to 31 May, from 3 to 4 June and from 8 to 9 June (compare Fig. 4a and d). To remove the wind noise, we subtract the seismic amplitude during the repose time from the seismic amplitude during the tremor pulses (Fig. 4c).

While the seismic amplitude increases linearly, the tremor pulse cycle duration changes often and rapidly. We use these changes to define six periods (cyan vertical lines on Fig. 3, 4 and Table 1). Period 1: The pulse cycle duration decreases from 13.1±3.5 min to 8±3 min on 3 May (Fig. 4f) and then remains stable. Period 2: The pulse cycle duration suddenly increases to 14±1 min at 4:22 on 5 May. Within 8 hours it decreases to 7.5±0.5 min and linearly increases to 9.7±0.4 min at 9:19 on 8 May. Period 3: Continuous tremor restarts and transitions to 17.2±0.8 min long pulses at 19:15. This tremor cycle duration shortens to 10.3±0.4 min on 9 May and linearly increases to 11.7±1 min on 10 May. Period 4: The cycle duration suddenly decreases to 8.5±0.3 min at 11:36 on 10 May and to 5.2±0.2 min at 16:00 on 11 May. The cycle duration then gradually increases to 7±0.2 min on 17 May at 17:30. Concurrently, cycles exist that are 3 min longer than the short cycles. Period 5: From 17 May at 17:30 to 10 June at 5:00 the duration increases from 7±0.2 to 15±0.4 min. At 5:00 on 10 June the tremor amplitude and cycle duration suddenly decrease and fluctuate between 5.4±1.5 and 10±3.4 min (Fig. 4f). Period 6: The pulse cycle duration decreases to a stable 3.5±0.5 min interval from 10:00 on 13 June.

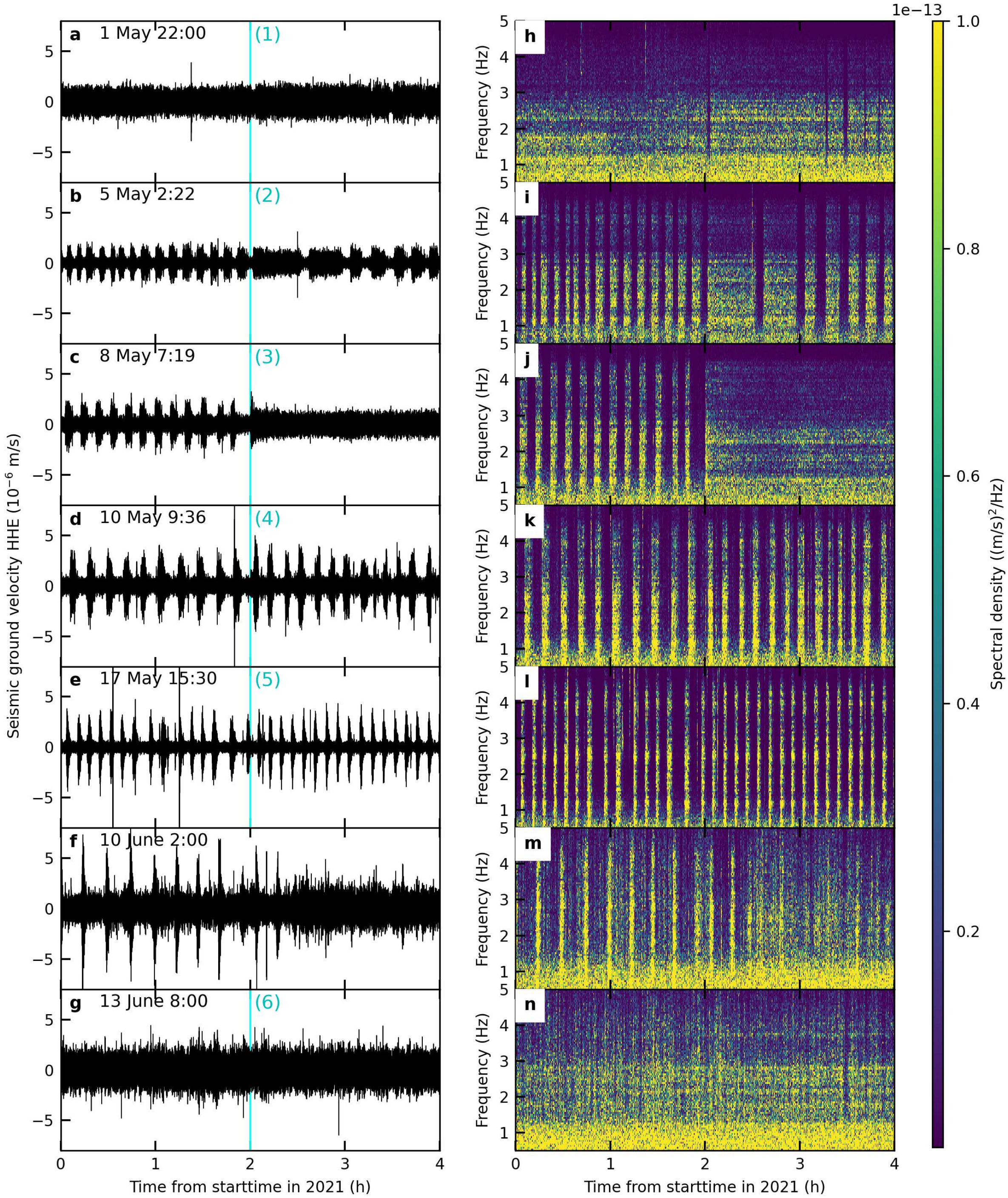

Figure 3: The seismic amplitude increased and frequency content became wider between 1 May and 14 June 2021. (a-g) 4 hour long seismograms of the east component of the seismometer. Date and time mark the start of the time window. The vertical cyan lines mark the changes in pulse pattern and the onset of the six periods. (h-n) 4 hour long spectrograms of subfigure a-f using a window length of 4096 samples and no overlap.

The pulse duration decreases exponentially from 11.4±3.2 min on 2 May to 5.5±2 min on 3 May (Fig. 4g). It then remains constant around 5.5 min until 10 May, although it is interrupted twice by longer pulse durations from 4:22 to 12:00 on 5 May and 19:15 to midnight on 8 May that mark the start of Periods 2 and 3, respectively. In Period 4 the

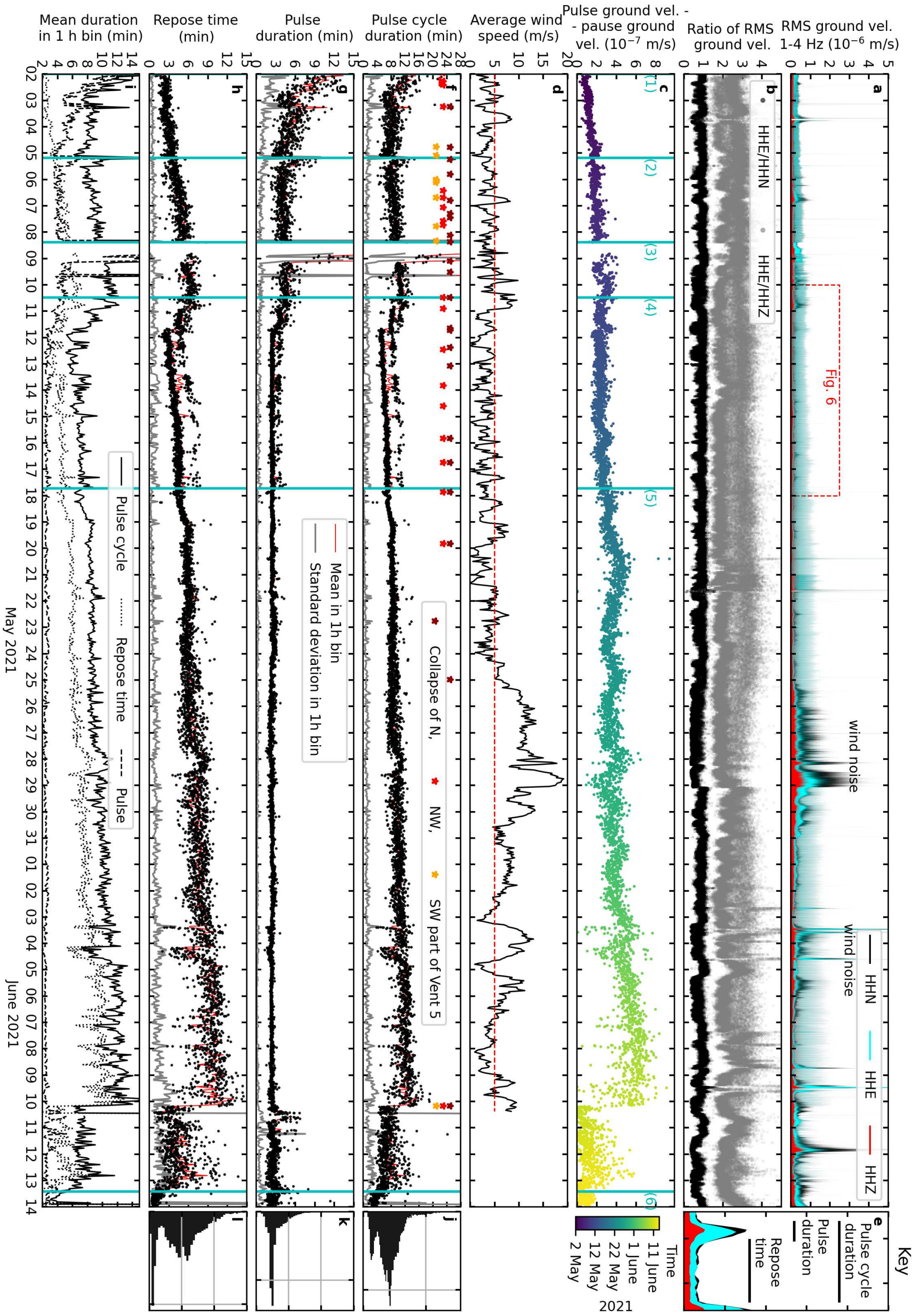

Figure 4: The pulse characteristics and repeating pattern changes with time. (a) RMS of the seismic ground velocity on all three components filtered 1 to 4 Hz. (b) Ratio of RMS seismic ground velocities HHE/HHN (black) and HHE/HHZ (grey). (c) Pulse ground velocity corrected for wind noise colored according to time. Cyan vertical lines mark the Periods 1 to 6. (d) Average wind speed measured by a weather station from IMO at Grindavik. The red horizontal line marks 5 m/s. (e) Key explaining cycle duration, pulse duration and repose time from 12:12 to 12:23 on 1 June. (f) Pulse cycle duration (black dots), the mean (red line) and standard deviation (grey line) in a 1 h long time window. Dark red, red and orange stars mark collapses of the northern, northwestern and southwestern part of the vent, respectively. (g) Same as subfigure f for pulse duration and (h) repose time. (i) Mean duration as in subfigures f-h. (j-l) Histograms of subfigures f-h.

pulse duration decreases abruptly at 11:36 on 10 May to 3.6±0.3 min and at 16:00 on 11 May to 2.6±0.2 min. In this period 3.6 min long pulses coexist with the dominant 2.6 min short ones. From 17 May in Period 5 the pulses duration is 2.5±0.1 min with standard deviations increasing to 0.5 min after 10 June. Tremor pulses become less visible after 10:00 on 13 June in Period 6 when continuous tremor dominates again.
From the start of Period 1 to the end of Period 3 the tremor repose time increases linearly from 1.7±0.6 min to 6.3±0.5 min (Fig. 4h). In Period 4, the repose time suddenly shortens to 4.6±0.7 min at 11:36 on 10 May and to 3.1±0.5 min at 16:00 on 11 May. From 11 May to 10 June, the repose time increases linearly to 11.3±2 min. In Period 4, the short repose times alternate with repose times which are 2 min longer than the short repose times. In Period 5, the longer repose times do not reappear. On 10 June the repose time decreases suddenly and fluctuates between 3.5±1.8 and 7.0±3.1 min. In Period 6, from 10:00 on 13 June continuous tremor restarts with weak fluctuations in amplitude.
In general, the eruption features long pulses and short repose times in early May, and short pulses and long repose times in mid June.

6.4 6 Periods in May and June with Different Fountaining Pattern

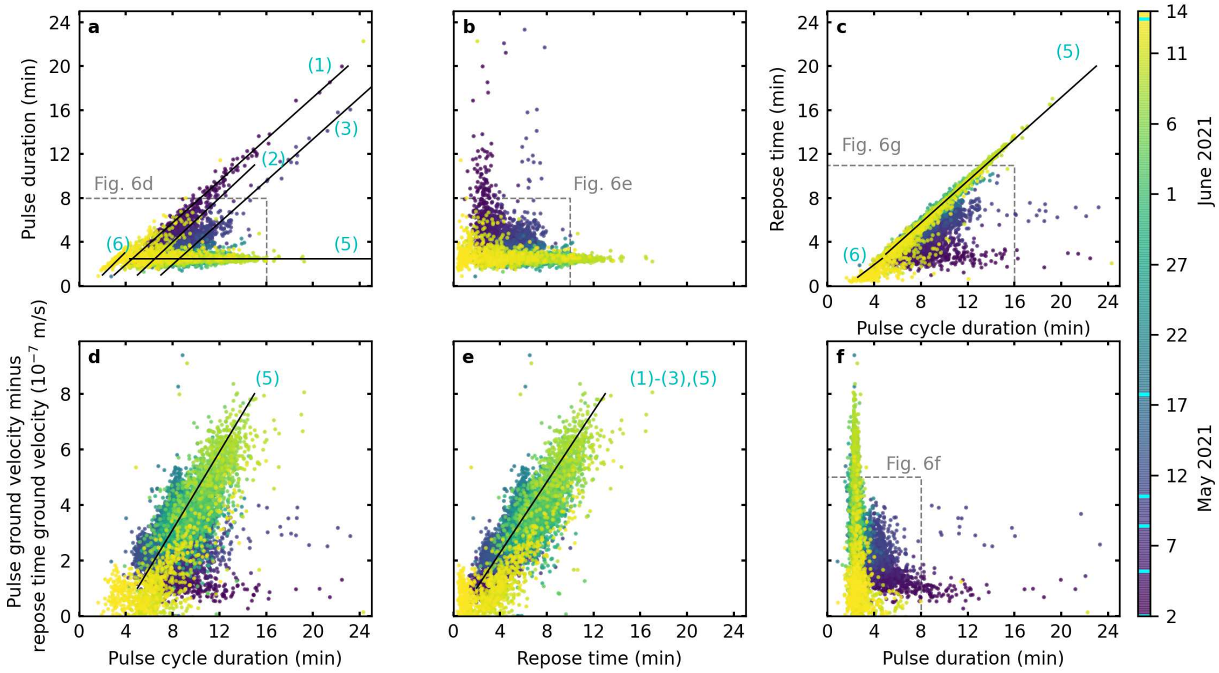

Figure 5: Six periods exist from 2 May to 14 June with different correlation patterns. (a-b) Correlation of pulse duration with (a) cycle duration and (b) repose time. Colors indicate the time. The labelled black lines highlight the correlation trends in Periods 1 to 3, 5 and 6 in all subfigures. (c) Correlation of repose time and cycle duration. (d-f) Correlation of pulse ground velocity corrected for wind noise and (d) cycle duration, (e) repose time and (f) pulse duration. Points in Period 4 lie in the grey dotted boxes (see also Fig. 6d-g).

Here we examine the relationship between the tremor pulse cycle duration, pulse duration, repose time and seismic tremor amplitude in the above mentioned periods (Fig. 4i, 5 and Fig.S3 to S8).
In Periods 1 to 3 (2 to 10 May), the cycle duration correlates with the pulse duration. A longer pulse cycle at the start of Period 1, 2 and 3 is hence due to a longer tremor pulse

duration (Fig. 4f and Fig. 5a). However, with time the pulse cycle gradually lengthens, primarily due to the linearly increasing repose time. Hence there is a weak correlation between the two parameters (Fig. S3c). The pulse duration and repose time do not correlate in Periods 1 to 3 (Fig. 5b).

In Period 5 (17 May to 13 June), the cycle duration correlates well with the repose time (Fig. 5c) but not with the pulse duration, which at this time is fairly constant (Fig. 5a and b). The collapse on 10 June does not affect this correlation. Period 6 starts on 13 June when cycle duration, pulse duration and repose time all correlate (Fig. 5a and c and Fig. S8a and c).

In Fig. 5d-f we compare the cycle duration, pulse duration and repose time with the seismic amplitude corrected for wind noise. In Periods 1-3 and 5 the mean pulse amplitude correlates with the repose time, i.e. larger amplitude tremor pulses are followed by longer pauses to the next pulse (Fig. 5e). Given the correlation between repose time and cycle duration in Period 5, it follows that the seismic amplitude and pulse cycle duration correlate in Period 5 (yellow points in Fig. 5d). No correlation exists between the amplitude and the pulse duration for all periods (Fig. 5f) and the pulse cycle duration in Periods 1 to 4 (blue points in Fig. 5d).

6.5 Coexisting Short and Long Pulses in Period 4

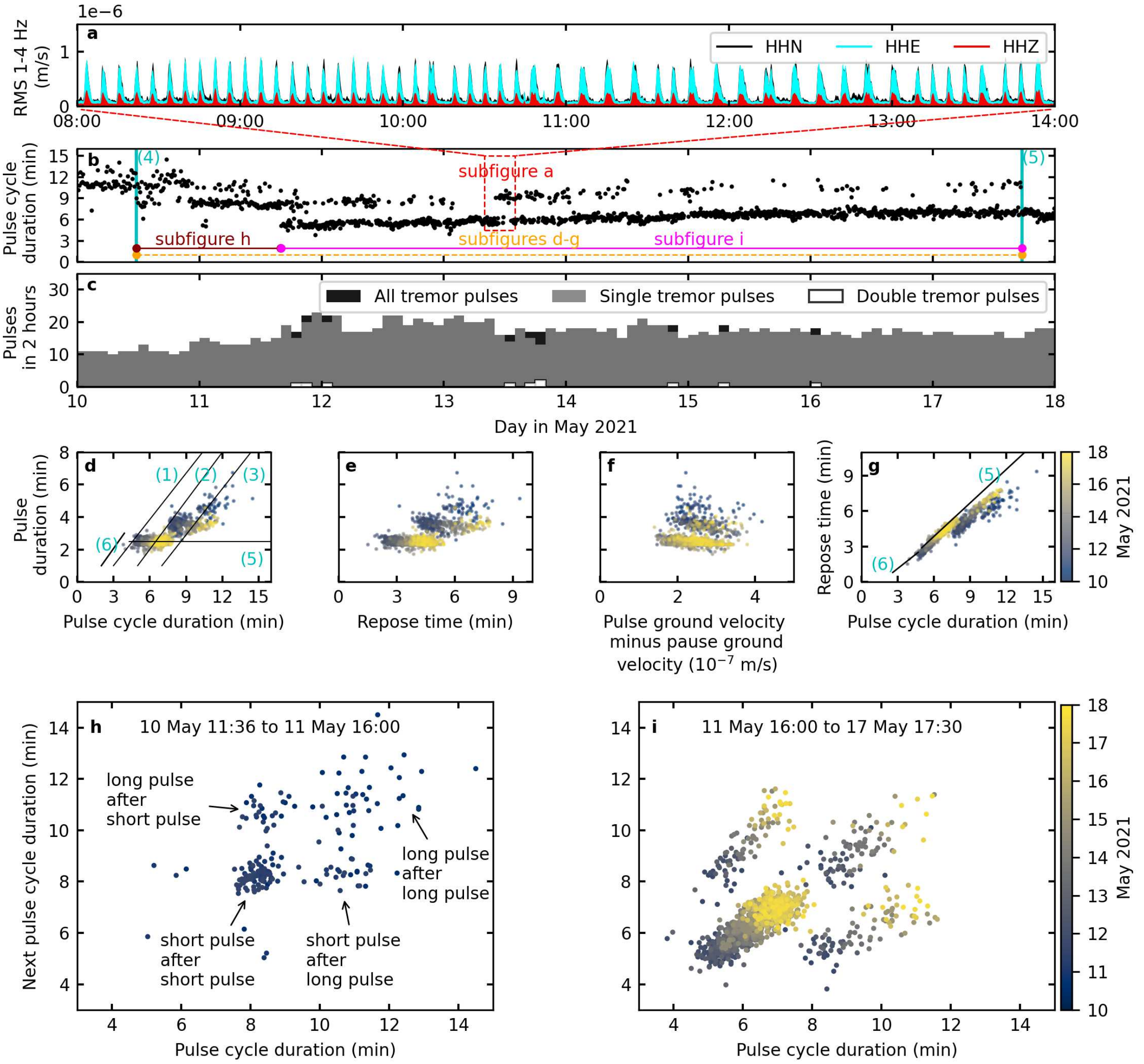

Figure 6: Short and long pulses followed by short and long repose times, respectively, coexist in Period 4 from 11:36 on 10 May to 17:30 on 18 May 2021. (a) Same as Fig. 4a zoomed in on 13 May from 8:00 to 14:00. (b) Dots and lines as Fig. 4f zoomed in from 10 to 18 May. The orange, horizontal line indicates the interval plotted in subfigures d-g. The dark red and magenta lines mark the intervals in subfigures h and i, respectively. (c) Number of pulse cycles per 2 hours where all cycles (black), 1589 short cycles starting with one pulse (grey) and 10 long cycles starting with two pulses (white) are highlighted. (d-g) Correlation of pulse duration and (d) pulse cycle duration, (e) repose time and (f) pulse ground velocity corrected for wind noise colored according to time. (g) Correlation of repose time and pulse cycle duration. Black lines as in Fig. 5. (h-i) Poincaré plot where the pulse cycle duration is plotted vs. the next pulse cycle duration from (h) 11:36 on 10 May to 16:00 on 11 May and from (i) 16:00 on 11 May to 17:30 17 May.

In Period 4 (10 to 17 May) the cycle duration, the pulse duration and the repose time decrease twice (Fig. 4f-h and Fig. 6b). As the pulse cycles become shorter from 10 towards 12 May, the number of cycles within a two hour time interval double (Fig. 6c). After 13 May the number of pulse cycles decreases, because the cycle duration increases.
Following the sudden decreases in cycle duration, short and longer pulse cycles coexist

(Fig. 6a and b). Another interesting feature of individual cycles is that short repose times follow short pulses, and longer repose times follow longer pulses (Fig. 6a and e). The cycle duration, pulse duration and repose time all correlate in Period 4 (Fig. 6d, e and g). However, the seismic amplitude is not systematically affected by the pulse duration (Fig. 6f) or the repose time.

Ten of the longer pulses consist of two amplitude peaks separated by an amplitude decrease of at least 50% of the maximum. In all other cases we could not distinguish separate peaks (Fig. 6a). We refer to pulses with one and two clear peaks as single and double pulses, respectively (Fig. 6c). While the two peaks in a double pulse have around 1 min temporal spacing, the following cycle persists 8 to 10 min. For single pulses most cycles last 5 to 7 min (Fig. 6h and i). The double pulses appear between 11 and 16 May and are most dominant on 11 and 13 May (Fig. 6c).

We assess the temporal sequence of short and long pulse cycles using a Poincaré plot (Fig. 6h and i). 76% of all pulses are short, while 24% of all pulses are long. The number of occurrences where a short pulse follows a long one is identical to the number of occurrences of a long pulse following a short one. 76% of the short pulses are followed by a short pulse and 61% of the long pulses are followed by a long pulse. 47%, 15%, 15% and 23% of the sequences are short-short, short-long, long-short and long-long, respectively. The sudden shortening and slow increase of the pulse cycle duration do not affect this sequence (Fig. 6i). Poincaré plots of all periods are shown in Fig. S9.

7 Discussion

7.1 Magmatic Processes and Episodic Venting of Magma

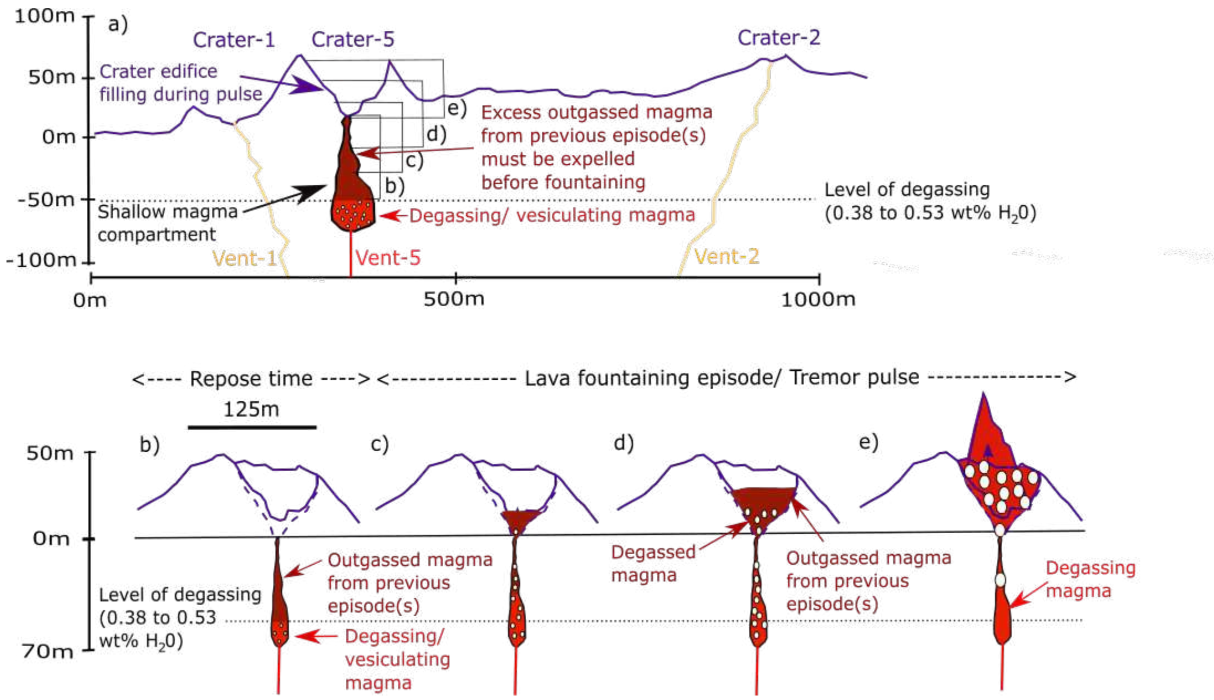

Figure 7: Temporal evolution of lava effusion during a tremor pulse. (a) Summarising the steps of lava effusion (b-e) in the context of the other vents not effusing lava in May. (b) In the repose time, undegassed magma (red) accumulates beneath a cap of outgassed magma (dark red). (c-d) During the pulse, the outgassed magma is pushed upwards into the crater by the undegassed magma. (e) During fountaining the crater is full of hot and at this time degassing magma. Note that most of the volume is taken up by bubbles.

The magma erupted at Fagradalsfjall is basaltic, with a whole rock composition containing 47.1 to 49.8 wt% SiO_2 and 8.6 to 9.7 wt% MgO. Its water content ranges from 0.38 to 0.53 wt% (Bindeman et al., 2022). The estimated magma source depth ranges from 10 to 17 km or from a magma reservoir within the lower crust (Halldórsson and al, 2022; Hobé et al., 2022). The solubility of CO_2 and H_2O in magma is linked, so the more CO_2 is in the magma, the less it contains of H_2O and vice versa. As basaltic magma rises from its storage reservoir, CO_2 begins to degas from the magma, and the magma becomes under saturated in H_2O, delaying its degassing until the magma is near the surface (Dixon et al., 1995; Dixon and Stolper, 1995).

In case of the Fagradalsfjall eruption, water began to degas from the magma at 1.5 MPa to 2.8 MPa pressure, equivalent to about 50 to 100 m depth (Newman and Lowenstern, 2002). Because of the very slow magma ascent rates in the Fagradalsfjall, with an average in the range of ∼0.02 m/s (Hobé et al., 2022), the degassing driving each episode is most likely driven by continuous bubble nucleation within the above-mentioned depth interval (Houghton and Gonnermann, 2008; Le Gall and Pichavant, 2016).

In early April, the magma discharge increased from about 5 to 10 m^3/s and consequently, new erupting vents open (Fig. 1). These modifications in the eruptive vent system increases the eruptive fissure length from 180 m to 600 m. This decreased the magma ascent speed from 0.03 m/s to 0.02 m/s (vent width remains 1 m). During this time the eruption featured open-vent activity and steady outpouring of lava. Drone-derived observations of bubbling magma in the vents along with high vesicularity (>70%) of erupted tephra clasts indicate that a two-phase flow (liquid and bubbes) had developed at the very top of the shallow conduit (Parfitt, 2004). The decompression rate was about 500 Pa/s.

On 1 and 2 May, the activity became confined to a single vent, Vent-5 (70 m-long and 1 m-wide crack; magma output $10\,m^3/s$). Consequently, the magma ascent speed increased to 0.14 m/s, bringing the eruption into the Hawaiian eruption field (per classification of Parfitt et al. (1995). This ascent rate indicates a minimum increase in decompression rate from 500 Pa/s in late April to 4000 Pa/s after 2 May. Degassing of H_2O and subsequent bubble nucleation and diffusion-driven bubble growth were the primary drivers of the eruptive activity at Fagradalsfjall (Sparks, 1978). Higher decompression rates promote more intense lava fountaining (Head and Wilson, 1987; Mangan et al., 2014; Parfitt, 2004; Parfitt and Wilson, 1994, 1995, 1999; Parfitt et al., 1995). Frequency and intensity of fountain episodes are driven by the amount of magma ready to degas at any one time (Mangan et al., 2014).

The free lava surface in the craters always fluctuated to a degree. However, it fluctuated most significantly after the activity became confined to Vent 5 and the eruption behavior was distinctly episodic – with magma rising to the brim of the crater at peak activity in each eruption episode and dropping below the crater floor in the repose time. The lava that drained back into the shallow conduit at the end of each episode was outgassed (i.e. lost gas and bubbles). When in the underlying container, it sits on top of the magma column filling the plumbing system that continually replenishes the shallow conduit from below by fluxing of fresh and undegassed magma (Fig. 7). With increasing proportions of fresh magma, the free surface of the outgassed magma is pushed upwards and the system experiences decompression which initiates degassing and vesiculation. Because of the low melt viscosity the bubbles nucleate easily, grow and rise rapidly, a process that lead to exponentially intensifying degassing from the newly arrived fresh magma (Fig. 7c) and formation of bubble strings as evident from development of (thermal) convection within the outgassed top of the magma column (Fig. 7d-e). Our observations show that the largest observed bubbles breaking the free surface within the crater had diameters of 20 to 50 m. This indicates bubble growth from sub-micron size to tens of meters within the magma during a rise of 50 to 100 m. This process of escalating degassing pushes the degassed lava out of the crater. This further enhances the decompression rates, which results in run-away vesiculation, such that bubbles occupy the largest volume fraction of the magma filling the crater, eventually driving the lava fountaining activity.

At the onset of lava fountaining the outgassing rates (gas is removed from the melt) start to exceed the rate of degassing (where gas moves into a bubble). This imbalance results in fountaining of waning intensity until this part of the system runs out of gas. Consequently, the fountaining comes to an abrupt halt, the magma volume in the crater collapses as the gas escapes and the outgassed magma drains rapidly into the underlying container.

7.2 Why did the Eruption become Episodic?

From the 5 to the end of April up to six conduits feed magma to the surface. Each of these vents features semi-steady activity where magma degassing produces a steady bubble stream in the topmost part of the conduit resulting in perpetual bubbling and outgassing in the vents and continuous outflow of lava. As the vents shut down one by one from 17 to 30 April, the remaining active vents accommodate the additional flux and the lava fountain heights increase accordingly. This change is particularly well captured by the evolution at Vent 5 from 23 to 30 April, which at that time is the main focus of

the continuous activity: The fountain height and intensity grow exponentially. Around 01:00 of 2 May, the activity at Vent 5 abruptly becomes episodic.
Around this time eruption spectators reported hearing a deep, loud, thumping noise coming from the region between Vents-1a/1b and Vent-5, which are about 100 m apart. Activity at Vents 1a/1b, which, as seen on timelapse videos, had been steadily dwindling for a few days, came to halt at this time. In light of these on-site observations and the short distance between the two vents, it is reasonable to conclude that the separation between the shallow conduits of Vent-1 and 5 collapses at this time on 2 May and forms the container that initiates and controls the rhythmic eruption behavior of Stage 2. This magma container increases the magma volume available for near-simultaneous degassing (and outgassing) in the shallowest part of the conduit system, compared to the 1-meter-wide dike-like conduits active during Stage 1.
It is likely that the major crater-rim collapse that took place on 30 April to 2 May aided the modulation to episodic behavior (Fig. S1). When the crater-rim collapses came to halt in the afternoon of 2 May, the tremor pulse duration had shortened and stabilised at 8±3 min.
Hence, we propose that the abrupt shift to episodic eruption behavior is due to the formation of the container at the top of the shallow conduit and its influence on degassing and outgassing processes. Other features, such as a steadily growing crater volume, periodic crater wall collapses, and the retainment and recycling of older outgassed magma are second order features, that produced punctuation-like (i.e. rim collapses) or gradual (rheology or geometrical) changes of the episodic rhythm. In the sections that follow, it is worthwhile to keep in mind that for the purpose of discussion we assume that the magma supply rate from the source reservoir and the amount of undegassed magma reaching the shallow conduit compartment are effectively unchanged throughout May and until 14 June.

7.3 Is the Change in Tremor Pulse Duration linked to an Evolving Shallow-Conduit Container?

On 2 May, the tremor pulse duration decreases exponentially. Similar pattern, but over a longer time span, was observed during the early stages of the 1983-2018 Pu'u 'O'o eruption in Hawai'i (Heliker and Mattox, 2003), when the duration of the tremor pulses decreased exponentially from 12 days to 0.5 days in the period from 1983 to 1986. Between 2 and 10 May, this exponential decrease in tremor pulse duration repeats three times during the Fagradalsfjall eruption. From 11 to 17 May the tremor pulse duration is stable at about 2.5 min, but with periodic punctuations of tremor pulses of longer duration. After that the longer pulses disappear altogether.
The pattern described above is interpreted as follows: The repeated periods of exponential decrease in tremor pulse duration between 2 and 10 May are linked to periods were the volume of residual degassed magma in the shallow-conduit container increases. This is reflected in the transition from fast and often changing pulse duration to stable pulse duration (Fig. 4g). We interpret this to indicate a stepwise growth/enlargement of the shallow-conduit container until 11 May.
Furthermore, such growth may produce disturbances that lead to partial collapses of the crater rim; for example at 8:03:52 on 8 May, when the southern rim partially collapses into the crater followed by a large collapse on the northern crater rim at 8:46:14. Between 9:09 to 9:17 significant amount of crater rim material slides into the crater and concurrently tremor transitions back to low amplitude, continuous tremor (Period 3, Fig. 4a and f).

Stable pulse duration as observed from 11 May, suggests that a similar volume of magma degases in each pulse/episode, indicating that the shallow-conduit container reached a semi-steady form by the 17 May, when the punctuated longer duration pulses stop. Periodic enlargement of the shallow-conduit container implies rather abrupt increases in accumulated magma volumes and consequently, abundance of gas available for degassing, which may explain the brief periods of decreasing tremor pulse duration.

On 10 and 11 May the tremor pulse duration changes from 11.7±1 min, to 8.5±0.3 min and finally 5.2±0.2 min long cycles within a 29 h period (Fig. 6). Since short and long pulses coexist in this time period, this might indicate an underlying 3.2 min long process in the shallow-conduit container that repeats two to four times. A partial collapse from the crater wall might reduce the threshold of the system for effusion, for example by releasing more of the outgassed magma from the vent. The variation in the fraction of outgassed magma retained in the vent, may lead to tremor pulses of different duration in Period 4. Other scenarios to explain the coexistence of short and long pulses such as a larger and a smaller shallow-conduit container seem unlikely due to the stable pattern of the pulse duration and repose time.

Surprisingly, the system remains stable for several weeks so that subtle changes in the behaviour can be observed. This might be due to the slow and steady effusion at 5 to 15 m^3/s Landmaelingar Islands (2021); University of Iceland (2021). In comparison, effusion rates up to 300 m^3/s were measured in the first few days of the Holuhraun eruption 2014/15 (Eibl et al., 2017a) where continuous outflow dominated the eruptive style. If the effusion rate is higher, the system is pressurised and the geometry evolves faster to a stable status.

Interestingly, the repose time and the pulse duration do not correlate. The only exception is Period 4 when longer pulses are followed by a longer repose time. Similarly, Heliker and Mattox (2003) found that neither the pause before nor the pause after eruption correlated with the eruption duration, during the Pu'u 'Ō'ō-Kūpaianaha eruption in 1983 to 1986, Hawaii.

7.4 Increasing Repose Time of Fountaining Episodes Linked to Magma Accumulation in Crater

Throughout Period 1 to 3 and most of Periods 4 and 5, the repose time increased linearly. Zobin (2013) reported a slowly increasing repose time between paroxysmal episodes on Etna over a few months, while tremor sources retreated to larger depths. At Piton de la Fournaise in 2007 the repose time of tremor pulses and collapses of the rock column systematically shortened (Michon et al., 2007). Alparone et al. (2003) observed a sudden increase in temporal spacing of paroxysms at Etna without clear drift in 2000. Moschella et al. (2018) reported temporal spacing of lava fountain episodes increasing from 5 to 20 days on Etna. However, the seismic amplitude did not increase systematically. Such systematic drift in behaviour can be due to geometrical changes in the shallow plumbing system, gas content or physical properties (Moschella et al., 2018). Spampinato et al. (2015) reported a linear increase in repose time of six fountaining episodes until it breaks down for the last four episodes in the sequence. They attribute this to faster magma transport and a more efficient degassing following stabilization of the shallow conduit. In our case, such an interpretation might mean that the system keeps evolving until at least 14 June. However, based on the pulse evolution we suggest that it becomes meta-stable on 11 May and fully stable on 17 May.

The repose time may have increased due to growth of the shallow-conduit container at the top of the shallow conduit. If the size of the shallow-conduit container increases with time, more magma is needed to fill it and to trigger fountaining. A volume increase in the shallow-conduit container is supported by the observation that the continually growing crater was filled to the brim with bubbly lava during each episode, despite growing in volume with time. Since the repose time shortens on 10/ 11 May and 10 June, the shallow-conduit container must decrease in size, perhaps due to partial collapses from the crater rim. This could also explain shorter pulses after collapses in Period 4. However, it is unlikely that the collapse material reaches the shallow-conduit container since the connection at the bottom of the crater is narrow.

Based on an analysis of 15 eruptions of different volcanoes, Dominguez et al. (2016) linked the median repose time of explosions within an eruption to the magma viscosity. Along these lines, the systematic increases in repose time that we report here might also relate to increases in the magma viscosity. Sudden decreases in repose time can then be caused by a viscosity decrease or be related to variations in the actual mass fraction of the degassed magma within the compartment or to variations in degree of cooling experienced by the magma as it circulates at the interface with the atmosphere. However, the empirical relationship by Dominguez et al. (2016) was developed based on the median repose time during one eruption. Hence, fast changes in repose time within one eruption described here would require fast changes in magma viscosity.

Similar to the hypothesis on viscosity, we suggest that the repose time is linked to the degassed lava volume that remains in the crater or the shallow-conduit compartment at the end of individual episodes (Fig. 7). The crater height increases fast from 10 May (Fig. 2a). It also increases in width and finally closes on all sides increasing the lava volume steadily. More lava could accumulate in the crater during an episode and consequently the volume of residual degassed magma increased. To start a new pulse, the increased volume of degassed lava needed to be cleared through and out of the crater, and thus may have increased the repose time from 10 May to 10 June (Fig. 4h). In this scenario decreases in repose time may have been caused by collapse material that blocks the vent between the crater and the shallow-conduit container. If a collapse happens when lava resides in the crater, then it may disturb the pressure condition within the underlying degassing magma. This may start - depending on the exact state of system and size of the collapse - a lava fountaining episode. This hypothesis is challenged by the fact that after some pulses the crater drains completely according to drone footage.

7.5 Coexistence of Short and Long Tremor Pulses

The random sequence of short and longer pulses reminds us of Strokkur geyser in south Iceland. In the case of the Fagradalsfjall eruption shorter pulses consist of 1 peak in seismic amplitude. Most of the longer pulses, however, consist of closely spaced peaks that merge into one and only for 10 pulses we detect two distinct separate peaks (Fig. 6.5a). We did not observe pulses containing three or more clear peaks. Similarly, the geyser Strokkur is characterised by single to sextuple eruptions, where sextuple eruptions are composed of six water fountains at an average temporal spacing of 16.1 s (Eibl et al., 2020). While 81% of the geyser eruptions are single eruptions, here we find that 76% of the pulses in Phase 4 of the Fagradalsfjall eruption are short. We hence find a similarity of number and duration of single and double eruptions at Strokkur and the Fagradalsfjall eruption. However, repose times for one eruption type at Strokkur are stable because there is no external or internal change in the system. Eibl et al. (2020) noted that the waiting time after eruptions linearly increases from single to sextuple eruptions. Similarly, longer pulses during the Fagradalsfjall eruption are followed by a longer repose time. While the geyser behaves repetitive, with no systematic change of eruption duration or frequency, the system at Fagradalsfjall evolved dynamically with time (Fig. 4f-h). While the geyser is a water-filled system driven by accumulating steam and superheated water, here the magma and the gas form a 2 phase system that is driven to eruption due to the H_2O exsolution from the magma. The underlying mechanisms are hence not comparable, but in Period 4 it might be the best analog we have.

7.6 Linear Increase in Seismic Amplitude

Assessing the seismic amplitude of one single tremor pulse, it coincides in time with lava overflow in Crater-5 and subsequent fountaining (Fig. 2b and c). Tremor starts when the lava level in the crater begins to rise, in many cases leading to an overflow. The tremor peaks when the lava fountaining reaches the highest intensity and it stops when fountaining stops (Fig. 2b and c). Observations suggest that at the beginning of an episode degassed, viscous magma is pushed out of the crater, followed by less viscous and degassing magma towards the end of the pulse. Similarly, a correlation between tremor pulse and lava fountaining height was reported from Etna, Italy (Alparone et al., 2003; Falsaperla et al., 2005; La Spina et al., 2015; Tanguy and Patane, 1984; Zobin, 2013), Alaska (McNutt, 1987) and Hawaii (Heliker and Mattox, 2003).
At Fagradalsfjall from 2 May to 14 June the peak seismic amplitude linearly increases and correlates with the repose time (Fig. 4c and h) but it never correlates with the pulse duration. Similarly, Alparone et al. (2003) observed no correlation between the fountaining duration and the seismic amplitude on Etna. La Spina et al. (2015) reported a correlation between longer repose times and stronger tremor amplitude during fountaining on Etna. Based on chemical data, they suggest that the shallow-conduit container feeding the eruption was gas overpressurised and that with time more CO_2-rich gas reached the shallow-conduit container while the repose time increased. However, we suggest here that the system is stable from 11 May and that the inflow from magma is stable from May to mid June.
The increase in seismic amplitude might be linked to the increase in height and width of Crater-5 and the thickening crater walls. However, after 10 June the seismic amplitude decreases after a major collapse on a circular fault inside the crater. This further increases the uppermost crater width and reduces the wall thickness while the seismic amplitude decreases. The inner width of the crater decreases due to accumulation of debris in lower parts of the crater. We observe that the fountain height also increases alongside the increase in seismic amplitude in early May. However, in the second half of May, the lava fountains transition from 300 m high, episodic fountaining (Fig. 1e), to slow starting, swelling lava overflow, followed by few meter high fountains (Fig. 1f). While the fountain height decreases from 18 May, the seismic amplitude keeps increasing. Hence, the crater shape and fountain height cannot explain the observed amplitude pattern.
However, the transition to swelling, vigorous overflow of magma out of the crater with minor regular lava fountains (Fig. 1f) reflects the accumulation of degassed magma in the shallow-conduit container. During Period 5, the degassing magma needs to go through liquid degassed magma that affects its ascent and decompression rate, reflected in greatly reduced lava fountain height. This magma might see more friction in the uppermost magma column leading to an increasing tremor amplitude. However, during the collapse on 10 June, the lava properties and composition remain stable, while the tremor amplitude decreases threefold (Fig. 3f).

In a review of 24 eruptions of 18 volcanoes, McNutt and Nishimura (2008) found a proportionality between the square-root of the cross-sectional vent area and the tremor amplitude in reduced displacement. For the Fagradalsfjall eruption this suggests that the collapse on 10 June reduces the vent dimensions, i.e. the cross sectional area of the active part of the eruptive vent. This interpretation suggests that the increasing seismic amplitude from 2 May to 10 June is due to increasing active vent dimensions. This is likely, and collapses from the crater rim in early May do not significantly affect the tremor amplitude possibly due to their small volume.
We suggest that the seismic amplitude is not linked to the fountain height, vent geometry or magma viscosity. Instead, we suggest that the dimensions of the eruptive vent govern the seismic amplitude. Episodic fountaining, steady magma flow and heat, mechanically erode and enlarge the vent and conduit. This reflects in larger seismic amplitudes as long as major collapses do not interfere with the vent dimensions. This enlarging vent might also explain the observed fountain height decrease from 17 May. However, it does not reduce the repose time since other factors contribute such as the degassed lava in the crater, the crater geometry and magma viscosity, and other parameters we do not have good control of.

8 Conclusion

We analyse the volcanic tremor behaviour recorded during the Fagradalsfjall eruption, Southwest Iceland from 19 March to 14 June 2021 using a seismometer (Stage 1 and the first half of Stage 2). From 2 May it features a tremor pulse pattern that evolves with time. We define six different periods based on the tremor pulse duration, tremor cycle duration and repose time pattern. The recorded tremor pulses coincide in time with episodes with up to 300 m high lava fountains.
For our analysis we assume that the magma composition, the magma supply rate and the amount of undegassed magma reaching the shallow crust is constant. In late April, the ascent velocity increases and Crater-5 partially collapses. In combination with an audible noise at the eruptive site on 2 May, we suggest that the preexisting shallow-conduit containers beneath Crater-1 and 5 merge. The formation influences the degassing and outgassing processes and starts the episodic lava fountaining phase.
Based on fast changes in the duration of lava fountaining episodes we suggest that the system grows and evolves until 11 May. It then reaches a steady state featuring regular tremor pulses. The repose time gradually increases from 2 May to 10 June, which we link to the increasing viscosity and amount of degassed magma that remains at the bottom of the crater, after a fountaining episode stops. Both the tremor pulse duration and repose time are affected by partial collapses of the crater. The collapsed material might block the vent that links the shallow-conduit container with the crater and disturb the pressure conditions of the system. Depending on the exact state of system and size of the collapse, this can start a lava fountaining episode. Based on our observations we also suggest that the vent is mechanically eroded with time and its dimensions increase so that it causes increasing seismic amplitudes and decreasing fountain heights.
We conclude that subtle changes in a shallow conduit system or shallow-conduit container are important to determine the behaviour of an eruptive system and to explain the seismic, volcanic tremor. We notice that the upper 100 m of the dike near the surface are critical, as this is the bubble forming region. Internal and external changes in crater geometry and height, magma viscosity, vent dimension change the boundary conditions of the system

and affect the fountaining pattern and frequency. This is possible during low-intensity eruptions with small effusion rates, but might also have implications for larger eruptions. The reported features can be further investigated in the context of modelling, detailed video camera data analysis, seismological tremor locations, or effusion rate or degassing studies.

9 Statements and Declarations

There are no competing interests.

10 Author contribution

Eva Eibl initiated the study conception and design. Data collection was performed and supported by Gylfi Páll Hersir, Egill Á. Gudnason, Thorbjörg Ágústsdóttir and Eva Eibl. Data analysis was performed by Eva Eibl, Thor Thordarson and Ármann Höskuldsson. The first manuscript draft was written by Eva Eibl and all authors commented on previous versions of the manuscript. All authors read and approved the final manuscript.

11 Acknowledgement

We thank Friðgeir Pétursson, Rögnvaldur Líndal Magnússon at ISOR and Daniel Vollmer at University of Potsdam for technical support in the field. We thank Sebastian Heimann for programming support, Sandeep for the kymograph images, and Undine Gnauck, Sarah Lindenlaub, Alea Joachim and Shaig Hamzaliyev for minor discussion and for creating and checking markers.

12 Data Availability

Seismic data from station NUPH are currently under an embargo and will be available via GEOFON in 2023. The list of tremor pulse start and end times is available at GFZ Data Services (Eibl et al., 2022).

13 References

Alparone, S., Andronico, D., Lodato, L., and Sgroi, T. (2003). Relationship between tremor and volcanic activity during the Southeast Crater eruption on Mount Etna in early 2000. *Journal of Geophysical Research: Solid Earth*, 108(B5):1–13.

Andronico, D., Cannata, A., Di Grazia, G., and Ferrari, F. (2021). The 1986–2021 paroxysmal episodes at the summit craters of Mt. Etna: Insights into volcano dynamics and hazard. *Earth-Science Reviews*, 220:103686.

Azzalini, A. and Bowman, A. W. (1990). A look at some geyser data from Old Faithful geyser. *Appl. Statist.*, 39(3):357–365.

Bindeman, I., Deegan, F., Troll, V., Thordarson, T., Höskuldsson, A., Moreland, W., Zorn, E., Shevchenko, A., and Walterr, T. (2022). Diverse mantle components with invariant oxygen isotopes in the 2021 Fagradalsfjall eruption, Iceland. *Nature Communications*.

Cannata, A., Catania, A., Alparone, S., and Gresta, S. (2008). Volcanic tremor at Mt. Etna: Inferences on magma dynamics during effusive and explosive activity. *Journal of Volcanology and Geothermal Research*, 178(1):19–31.

Carbone, D., Zuccarello, L., Messina, A., Scollo, S., and Rymer, H. (2015). Balancing bulk gas accumulation and gas output before and during lava fountaining episodes at Mt. Etna. *Scientific Reports*, 5.

Clifton, A. and Kattenhorn, S. (2006). Structural architecture of a highly oblique divergent plate boundary segment. *Tectonophysics*, 419:27–40.

Çubuk-Sabuncu, Y., Jónsdóttir, K., Caudron, C., Lecocq, T., Parks, M. M., Geirsson, H., and Mordret, A. (2021). Temporal Seismic Velocity Changes During the 2020 Rapid Inflation at Mt. Þorbjörn-Svartsengi, Iceland, Using Seismic Ambient Noise. *Geophysical Research Letters*, 48(11):1–10.

Dixon, J., Stolper, E., and Holloway, J. (1995). An experimental study of water and carbon dioxide solubilities in mid ocean ridge basaltic liquids. Part I: Calibration and solubility models. *Journal of Petrology*, 36:1607–1631.

Dixon, J. E. and Stolper, E. M. (1995). An experimental study of water and carbon dioxide solubilities in mid-ocean ridge basaltic liquids. Part II: Applications to degassing. *Journal of Petrology*, 36:1633–1646.

Dominguez, L., Pioli, L., Bonadonna, C., Connor, C. B., Andronico, D., Harris, A. J., and Ripepe, M. (2016). Quantifying unsteadiness and dynamics of pulsatory volcanic activity. *Earth and Planetary Science Letters*, 444:160–168.

Eibl, E. P., Bean, C. J., Jónsdóttir, I., Höskuldsson, A., Thordarson, T., Coppola, D., Witt, T., and Walter, T. R. (2017a). Multiple coincident eruptive seismic tremor sources during the 2014-2015 eruption at Holuhraun, Iceland. *Journal of Geophysical Research: Solid Earth*, 122(4):2972–2987.

Eibl, E. P., Bean, C. J., Vogfjörd, K. S., Ying, Y., Lokmer, I., Möllhoff, M., O'Brien, G. S., and Pálsson, F. (2017b). Tremor-rich shallow dyke formation followed by silent magma flow at Bárdarbunga in Iceland. *Nature Geoscience*, 10(4):299–304.

Eibl, E. P., Hainzl, S., Vesely, N. I. K., Walter, T. R., Jousset, P., Hersir, G. P., and Dahm, T. (2020). Eruption Interval Monitoring at Strokkur Geyser, Iceland. *Geophysical Research Letters*.

Eibl, E. P. S., Gnauck, U., Hamzaliyev, S., Hersir, G. P., Gudnasson, E., and Pétursson, F. (2022). Catalog of start and end times of lava fountaining episodes from 2 May to 14 June 2021 during the Fagradalsfjall eruption.

Falsaperla, S., Alparone, S., D'Amico, S., Grazia, G., Ferrari, F., Langer, H., Sgroi, T., and Spampinato, S. (2005). Volcanic tremor at Mt. Etna, Italy, preceding and accompanying the eruption of July - August, 2001. *Pure and Applied Geophysics*, 162(11):2111–2132.

Fischer, T., Hrubcová, P., Salama, A., Doubravová, J., Horálek, J., Ágústsdóttir, T., Gudnason, E. Á., and Hersir, G. P. (2022). Swarm seismicity illuminates stress transfer prior to the 2021 Fagradalsfjall eruption in Iceland. *Earth and Planetary Science Letters*.

Flóvenz, Ó. G., Wang, R., Hersir, G. P., Dahm, T., Hainzl, S., Vassileva, M., Drouin, V., Heimann, S., Isken, M., Gudnason, E. Á., Ágústsson, K., Ágústsdóttir, T., Horalek, J., Motagh, M., Walter, T., Rivalta, E., Jousset, P., Krawczyk, C., and Milkereit, C. (2022). One year of cyclic unrest in a hydrothermal field as a harbinger of a volcanic eruption. *Nature Geoscience*.

Geirsson, H., Parks, M., Vogfjörd, K., Einarsson, P., Sigmundsson, F., Jónsdóttir, K., Drouin, V., Ófeigsson, B. G., Hreinsdóttir, S., and Ducrocq, C. (2021). The 2020 volcano-tectonic unrest at Reykjanes Peninsula, Iceland: stress triggering and reactivation of several volcanic systems. In *EGU General Assembly Conference Abstracts*.

Gudmundsson, M. T., Jónsdóttir, K., Hooper, A., Holohan, E. P., Halldórsson, S. A., Ófeigsson, B. G., Cesca, S., Vogfjörd, K. S., Sigmundsson, F., Högnadóttir, T., Einarsson, P., Sigmarsson, O., Jarosch, A. H., Jónasson, K., Magnússon, E., Hreinsdóttir, S., Bagnardi, M., Parks, M. M., Hjörleifsdóttir, V., Pálsson, F., Walter, T. R., Schöpfer, M. P., Heimann, S., Reynolds, H. I., Dumont, S., Bali, E., Gudfinnsson, G. H., Dahm, T., Roberts, M. J., Hensch, M., Belart, J. M., Spaans, K., Jakobsson, S., Gudmundsson, G. B., Fridriksdóttir, H. M., Drouin, V., Dürig, T., Adalgeirsdóttir, G., Riishuus, M. S., Pedersen, G. B., Van Boeckel, T., Oddsson, B., Pfeffer, M. A., Barsotti, S., Bergsson, B., Donovan, A., Burton, M. R., and Aiuppa, A. (2016). Gradual caldera collapse at Bárdarbunga volcano, Iceland, regulated by lateral magma outflow. *Science*, 353(6296):262.

Halldórsson, S. A. and al, E. (2022). Rapid source shifting of a deep magmatic system revealed by the Fagradalsfjall eruption, Iceland. *Nature*.

Head, J. W. and Wilson, L. (1987). Lava fountain heights at Pu'u 'O'o, Kilauea, Hawaii: Indicators of amount and variations of exsolved magma volatiles. *Journal of Geophysical Research: Solid Earth*, 92(B13):13715–13719.

Heimann, S., Kriegerowski, M., Isken, M., Cesca, S., Daout, S., Grigoli, F., Juretzek, C., Megies, T., Nooshiri, N., Steinberg, A., Sudhaus, H., Vasyura-Bathke, H., Willey, T., and Dahm, T. (2017). Pyrocko - An open-source seismology toolbox and library. V. 0.3. Technical report, GFZ.

Heliker, C. and Mattox, T. N. (2003). The First Two Decades of the Pu'u 'Ō'ō-Kūpaianaha eruption: Chronology and Selected Bibliography. *U.S. Geological Survey Professional Paper*.

Hobé, A., Bazargan, M., Selek, B., Tryggvason, A., Group, S. S., and Gudmundsson, A. (2022). Quantifying the volcanotectonic parameters of the 2021 Fagradalsfjall eruption, Iceland. *Bulletin of Volcanology*.

Houghton, B. F. and Gonnermann, H. M. (2008). Basaltic explosive volcanism: Constraints from deposits and models. *Chemie der Erde - Geochemistry*, 68(2):117–140.

Icelandic Meteorological Office (2021). A minor eruption underway.

Jakobsson, S., Jónasson, K., and Sigurdsson, L. (2008). The three igneous rock series of Iceland. *Jökull*, 58:117–138.

Jakobsson, S., Jónsson, J., and Shido, F. (1978). Petrology of the Western Reykjanes Peninsula, Iceland. *J. Petrol.*, 19(4):669–705.

Jonsdottir, K., Sabuncu, Y. C., Geirsson, H., Klaasen, S., Caudron, C., Lecocq, T., Barsotti, S., Barnie, T., Sigmundsson, F., Oddsson, B., and Others (2021). Seismic Monitoring of the 2021 Fagradalsfjall Eruption, SW Iceland. In *AGU Fall Meeting 2021*. AGU.

Jonsson, J. (1983). Eldgos á sögulegum tíma á Reykjanesi (in Icelandic). *Náttúrufræðingurinn*, 52:127–174.

Kumagai, H., Ohminato, T., Nakano, M., Ooi, M., Kubo, A., Inoue, H., and Oikawa, J. (2001). Very-long-period seismic signals and caldera formation at Miyake Island, Japan. *Science*, 293(5530):687–690.

La Spina, A., Burton, M., Allard, P., Alparone, S., and Muré, F. (2015). Open-path FTIR spectroscopy of magma degassing processes during eight lava fountains on Mount Etna. *Earth and Planetary Science Letters*, 413:123–134.

Landmaelingar Islands (2021). Umbrotasvaedid á Reykjanesskaga.

Langer, H., Falsaperla, S., Masotti, M., Campanini, R., Spampinato, S., and Messina, A. (2009). Synopsis of supervised and unsupervised pattern classification techniques applied to volcanic tremor data at Mt Etna, Italy. *Geophysical Journal International*, 178(2):1132–1144.

Le Gall, N. and Pichavant, M. (2016). Homogeneous bubble nucleation in H2O- and H2O-CO2-bearing basaltic melts: Results of high temperature decompression experiments. *Journal of Volcanology and Geothermal Research*, 327:604–621.

Mangan, M., Cashman, K., and Swanson, D. (2014). The Dynamics of Hawaiian-style eruptions: A century of study. In Poland, M., Takahashi, T., and Landowski, C., editors, *Characteristics of Hawaiian Volcanoes*. USGS professional paper 1801.

McNutt, S. R. (1987). Volcanic tremor at Pavlof Volcano, Alaska, October 1973-April 1986. *Pure and Applied Geophysics PAGEOPH*, 125(6):1051–1077.

McNutt, S. R. and Nishimura, T. (2008). Volcanic tremor during eruptions: Temporal characteristics, scaling and constraints on conduit size and processes. *Journal of Volcanology and Geothermal Research*, 178(1):10–18.

Michon, L., Staudacher, T., Ferrazzini, V., Bachèlery, P., and Marti, J. (2007). April 2007 collapse of Piton de la Fournaise: A new example of caldera formation. *Geophysical Research Letters*, 34(21).

Moschella, S., Cannata, A., Di Grazia, G., and Gresta, S. (2018). Insights into lava fountain eruptions at mt. Etna by improved source location of the volcanic tremor. *Annals of Geophysics*, 61(4).

Munoz-Saez, C., Manga, M., Hurwitz, S., Rudolph, M. L., Namiki, A., and Wang, C. Y. (2015). Dynamics within geyser conduits, and sensitivity to environmental perturbations: Insights from a periodic geyser in the El Tatio geyser field, Atacama Desert, Chile. *Journal of Volcanology and Geothermal Research*, 292:41–55.

Newman, S. and Lowenstern, J. B. (2002). VolatileCalc: a silicate melt–H2O–CO2 solution model written in Visual Basic for excel. *Computers and Geosciences*, 28(5):597–604.

Parfitt, E. (2004). A discussion of the machanisms of explosive basaltic eruptions. *Journal of Volcanology and Geothermal Research*, 134:77 – 107.

Parfitt, E. and Wilson, L. (1994). Pu' u 'O'o eruption of Kilauea volcano, Hawaii: a study of dike geometry and eruption mechanisms for a long-lived eruption. *J. Volcanol. Geotherm. Res.*, 59:179– 205.

Parfitt, E. and Wilson, L. (1995). Explosive volcanic eruptions IX. The transition between Hawaiian-style lava fountaining and Strombolian explosive activity. *Geophys. J. Int.*, 121:226– 232.

Parfitt, E. and Wilson, L. (1999). A Plinian treatment of fallout from Hawaiian lava fountains. *J. Volcanol. Geotherm. Res.*, 88:67–75.

Parfitt, E., Wilson, L., and Neal, C. (1995). Factors influencing the height of Hawaiian lava fountains: implications for the use of fountain height as an indicator of magma gas content. *Bull. Volcanol.*, 57:440–450.

Patrick, M. R., Orr, T., Wilson, D., Dow, D., and Freeman, R. (2011). Cyclic spattering, seismic tremor, and surface fluctuation within a perched lava channel, Kīlauea Volcano. *Bulletin of Volcanology*, 73(6):639–653.

Payne, R. (2021). The growth of the volcano at Geldingadalir.

Pedersen, G. B. M., Belart, J. M. C., Óskarsson, B. V., Gudmundsson, M. T., Gies, N., Högnadóttir, T., Hjartardóttir, Á. R., Pinel, V., Berthier, E., Dürig, T., Reynolds, H. I., Hamilton, C. W., Valsson, G., Einarsson, P., Ben-Yehosua, D., Gunnarsson, A., and Oddsson, B. (2022). Volume, effusion rate, and lava transport during the 2021 Fagradalsfjall eruption: Results from near real-time photogrammetric monitoring. *Geophysical Research Letters*.

Privitera, E., Sgroi, T., and Gresta, S. (2003). Statistical analysis of intermittent volcanic tremor associated with the September 1989 summit explosive eruptions at Mount Etna, Sicily. *Journal of Volcanology and Geothermal Research*, 120:235–247.

Sæmundsson, K. and Sigurgeirsson, M. Á. (2013). The Reykjanes Peninsula. In Sólnes, J., Sigmundsson, F., and Bessason, B., editors, *Natural hazards in Iceland, volcanic eruptions and earthquakes (in Icelandic).*, pages 379–401. Viðlagatrygging Íslands/Háskólaútgáfan, Reykjavík.

Sæmundsson, K., Sigurgeirsson, M. Á., and Friðleifsson, G. Ó. (2020). Geology and structure of the Reykjanes volcanic system, Iceland. *Journal of Volcanology and Geothermal Research*, 391:106501.

Sigmundsson, F., Parks, M., Hooper, A. J., Geirsson, H., Vogfjörd, K. S., Drouin, V., Ofeigsson, B., Hreinsdottir, S., Hjaltadottir, S., Einarsson, P., Jonsdottir, K., and Barsotti, S. (2021). Un-stressing of crust prior to eruptions: Precursors to the 2021 eruption at Geldingadalir, Mt. Fagradalsfjall, in the Reykjanes Peninsula Oblique Rift, Iceland. In *AGU Fall Meeting 20212*.

Sigurgeirsson, M. Á. (1995). The Younger-Stamp ar eruption at Reykjanes, SW-Iceland. *Náttúrufræðingurinn*, 64:211–230.

Spampinato, L., Sciotto, M., Cannata, A., Cannavó, F., La Spina, A., Palano, M., Salerno, G. G., Privitera, E., and Caltabiano, T. (2015). Multiparametric study of the February-April 2013 paroxysmal phase of Mt. Etna New South-East Crater. *Geochemistry, Geophysics, Geosystems*, 16(6):1932–1949.

Sparks, R. S. J. (1978). The dynamics of bubble formation and growth in magmas: A review and analysis. *Journal of Volcanology and Geothermal Research*, 3(1):1–37.

Swanson, D. A., Duffield, W. A., Jackson, D. B., and Peterson, D. W. (1979). Chronological narrative of the 1969-71 Mauna Ulu eruption of Kilauea Volcano, Hawaii. *U.S. Geological Survey Professional Paper 1056*, 1056:55 p.

Tanguy, J. C. and Patane, G. (1984). Activity of Mount Etna, 1977-1983: Volcanic Phenomena and Accompanying Seismic Tremor. *Bulletin of Volcanology*, 47-2(2).

Tepp, G., Hotovec-Ellis, A., Shiro, B., Johanson, I., Thelen, W., and Haney, M. M. (2020). Seismic and geodetic progression of the 2018 summit caldera collapse of Kīlauea volcano. *Earth and Planetary Science Letters*, 540.

Thompson, G., McNutt, S. R., and Tytgat, G. (2002). Three distinct regimes of volcanic tremor associated with the eruption of Shishaldin Volcano, Alaska 1999. *Bulletin of Volcanology*, 64(8):535–547.

Thordarson, T. and Höskuldsson, Á. (2008). Postglacial volcanism in Iceland. *Jökull*, 58:197–228.

Trnkoczy, A. (2012). Understanding and parameter setting of STA/LTA trigger algorithm. *New manual of seismological observatory practice 2*, pages 1–41.

University of Iceland (2021). Eldgos í Fagradalsfjalli.

Witt, T. and Walter, T. R. (2017). Video monitoring reveals pulsating vents and propagation path of fissure eruption during the March 2011 Pu'u 'Ō'ō eruption, Kilauea volcano. *Journal of Volcanology and Geothermal Research*, 330:43–55.

Zobin, V. M. (2013). *Complex monitoring of volcanic activity : methods and results*. Nova Science Publishers Inc.

Zobin, V. M. (2017). Volcanic Tremor. *Introduction to Volcanic Seismology*, 4:263–288.

14 Attachment

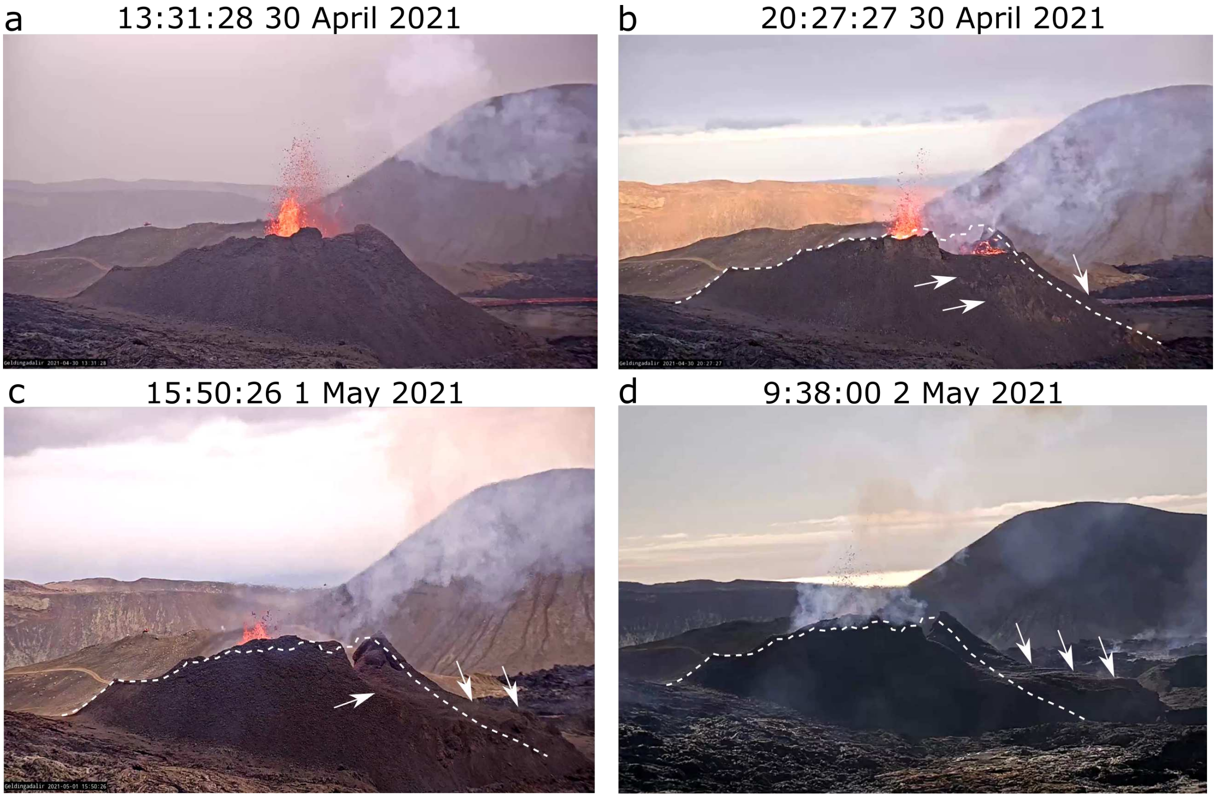

Figure S1: Partial collapse of Crater-5 from 30 April to 2 May 2021 viewed from Fagradalsfjall towards the southeast. Photos from a mbl.is camera at (a) 13:31:28 on 30 April shortly before the collapse started. Photos during the collapse at (b) 20:27:27 on 30 April, (c) 15:50:26 on 1 May and (d) 9:38:00 on 2 May. The crater outline from subfigure a is shown as white dashed line in subfigures b to d. White arrows highlight the collapse mass.

Unit: min	Period 1	Period 2	Period 3	Period 4	Period 5	Period 6
Start time	0:00 on 2 May	4:22 on 5 May	19:15 on 8 May	11:36 on 10 May	17:30 on 17 May	10:00 on 13 June
End time	4:22 on 5 May	19:15 on 8 May	11:36 on 10 May	17:30 on 17 May	10:00 on 13 June	
Cycle duration Trend	13.1±3.5 to 8±3 exponential	14±1 to 7.5±0.5 exponential 7.5±0.5 to 9.7±0.4 linear	17.2±0.8 to 10.3±0.4 exponential 10.3±0.4 to 11.7±1 linear	11.7±1 to 8.5±0.3 to 5.2±0.2 sudden drop 5.2±0.2 to 7±0.2 linear coexisting 3 min longer ones	7±0.2 to 15±0.4 linear from 10 June: 5.4±1.5 to 10±3.4	3.5±0.5 stable
Pulse duration Trend	11.4±3.2 to 5.5±2 exponential 5.5±2 stable	14.9±10.2 to 5.5±2 exponential 5.5±2 stable	24.3±11.9 to 5.5±2 exponential 5.5±2 stable	5.5±2 to 3.6±0.3 to 2.6±0.2 sudden drop 2.6±0.2 stable coexisting 1 min longer ones	2.5±0.1 to 2.5±0.5 stable	2.5±0.5 stable
Repose time Trend	1.7±0.6 to 6.3±0.5 linear			6.3±0.5 to 4.6±0.7 to 3.1±0.5 sudden drop 3.1±0.5 to 11.3±2 linear coexisting 2 min longer ones	3.1±0.5 to 11.3±2 linear from 10 June: 3.5±1.8 to 7.0±3.1	1±0.4 stable

Table 1: Overview of pulse cycle duration, pulse duration and repose times in all six periods. The values indicate the mean ± one standard deviation in 1 h time windows (Fig. reffig:drifting pulse behaviouri). Two values in one row denote a transition from the first to the second value while the trend in the line below describes the transition. If the trend changes during one period, this is noted with values and a trend in the third and fourth line of the respective box.

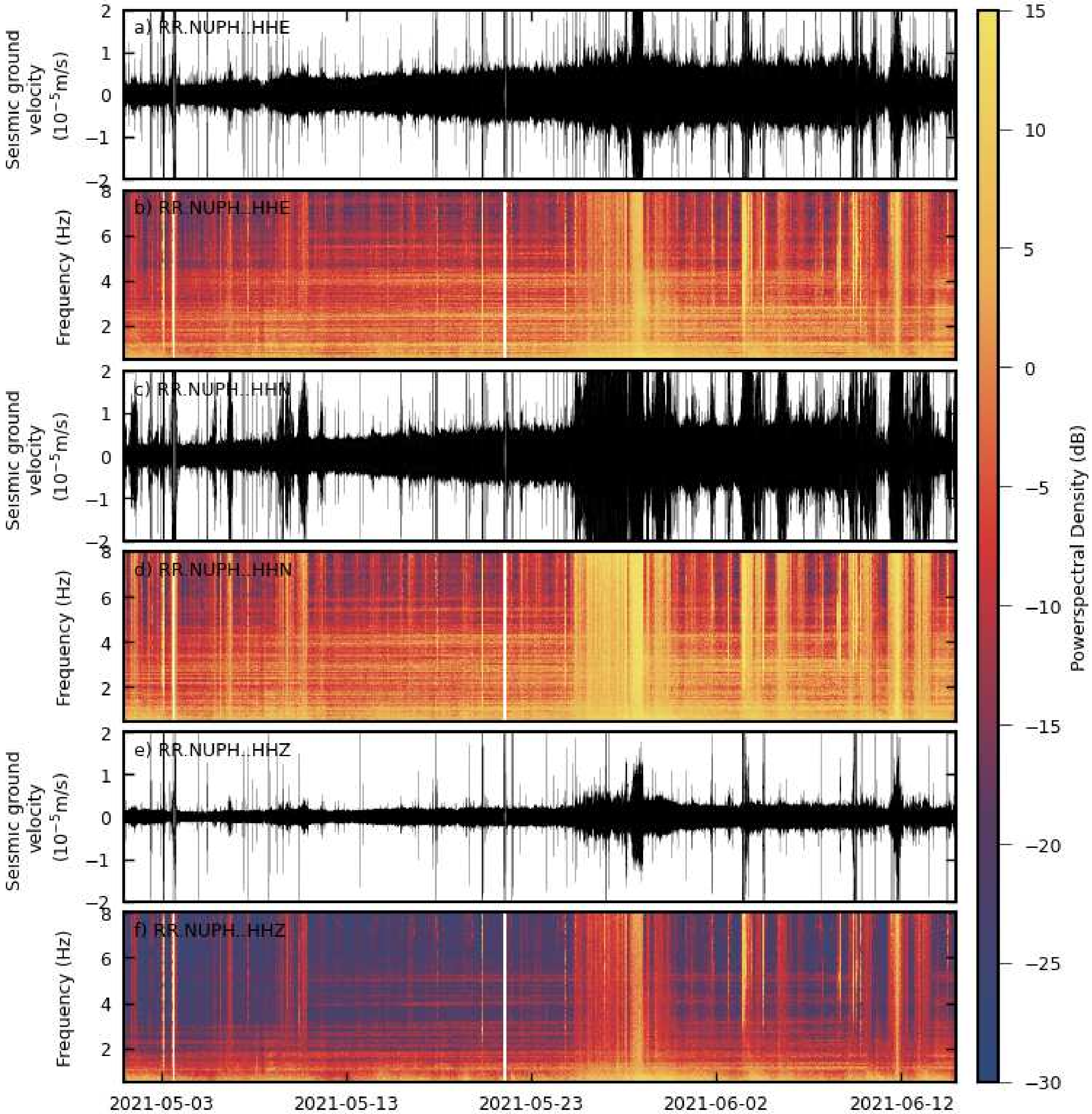

Figure S2: Tremor amplitude increase and widening frequency content from 1 May to 14 June 2021. (a) Seismogram and (b) power spectrogram using a moving 3600 s long time window with 50% overlap of the east component. (c and d) Same as subfigures a and b for the north component. (e and f) Same as subfigures a and b for the vertical component.

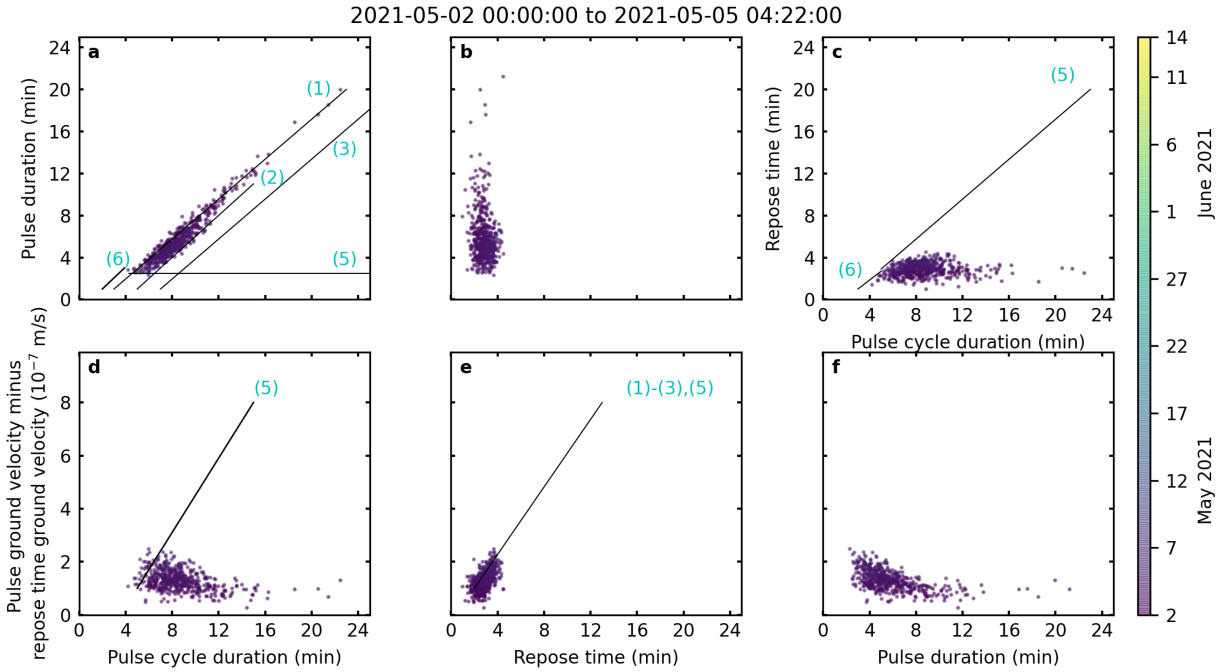

Figure S3: Same as Fig. 5 for points in Period 1.

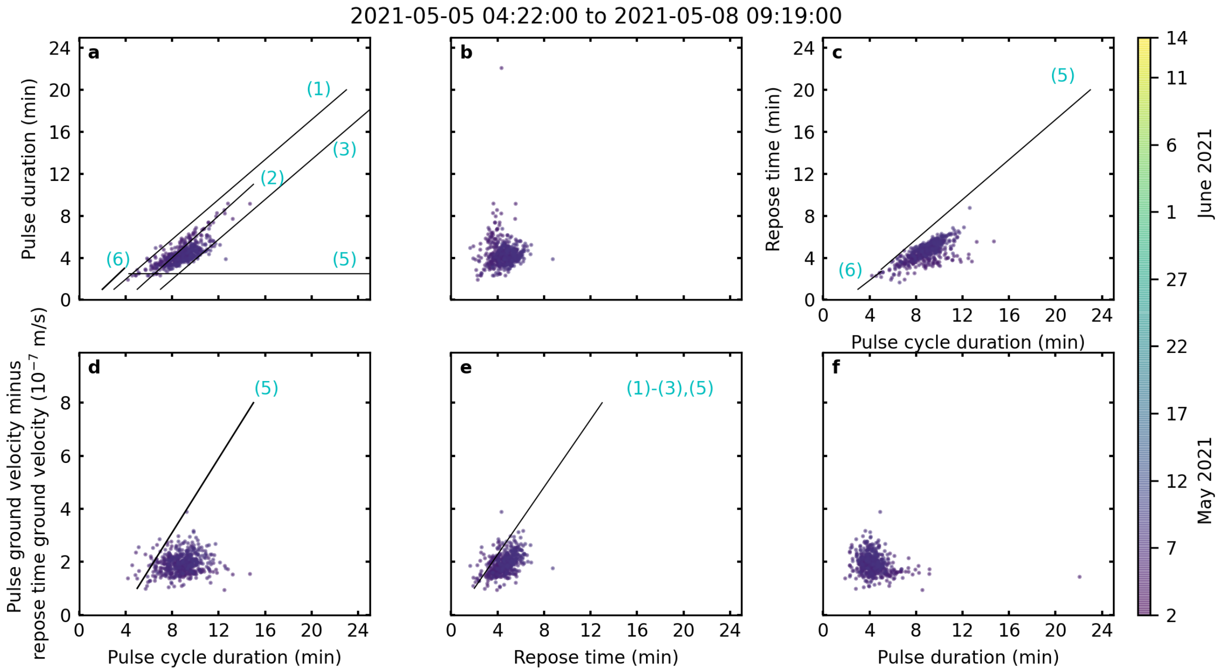

Figure S4: Same as Fig. 5 for points in Period 2.

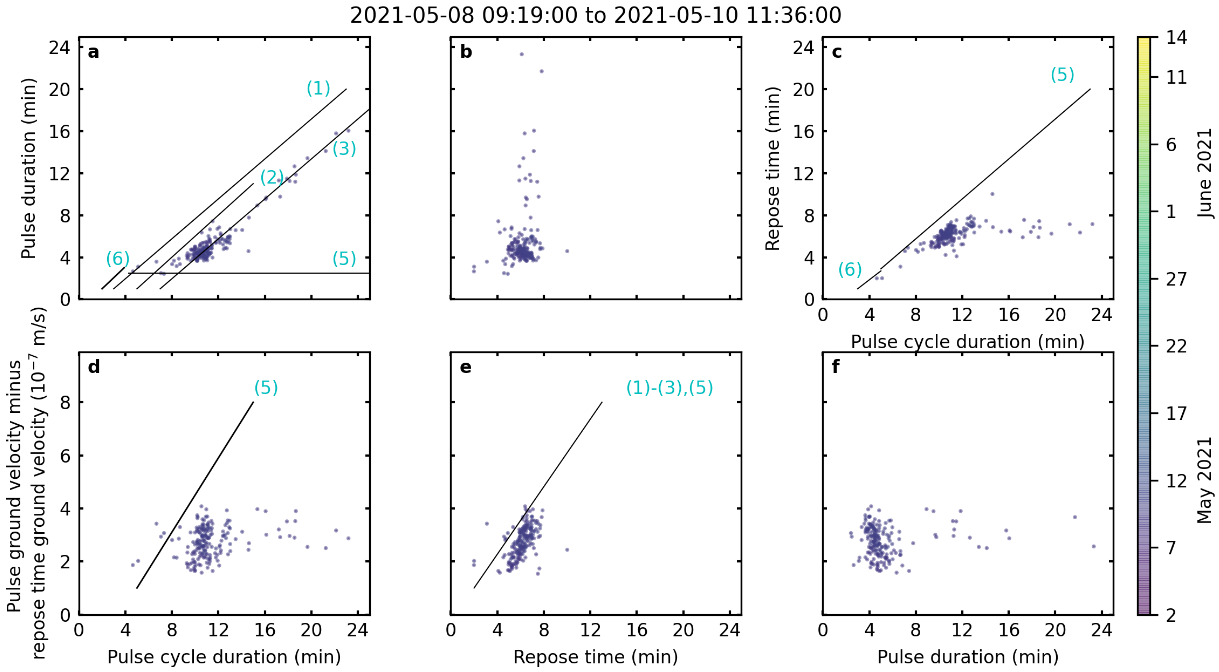

Figure S5: Same as Fig. 5 for points in Period 3.

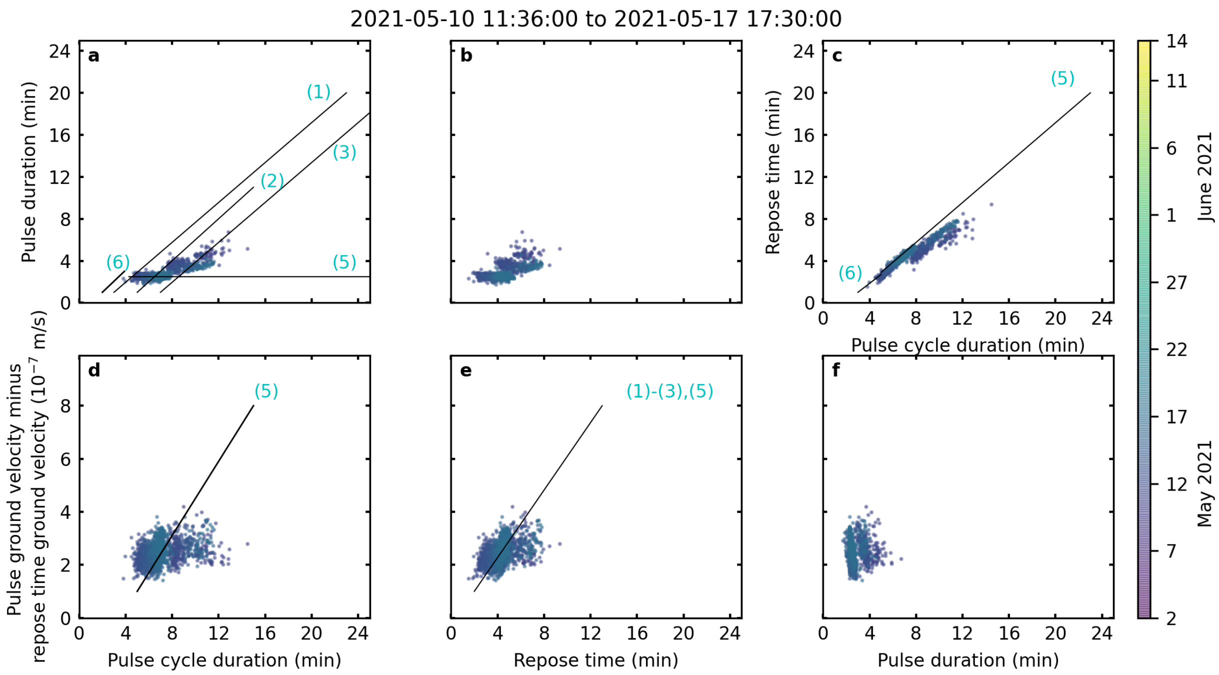

Figure S6: Same as Fig. 5 for points in Period 4.

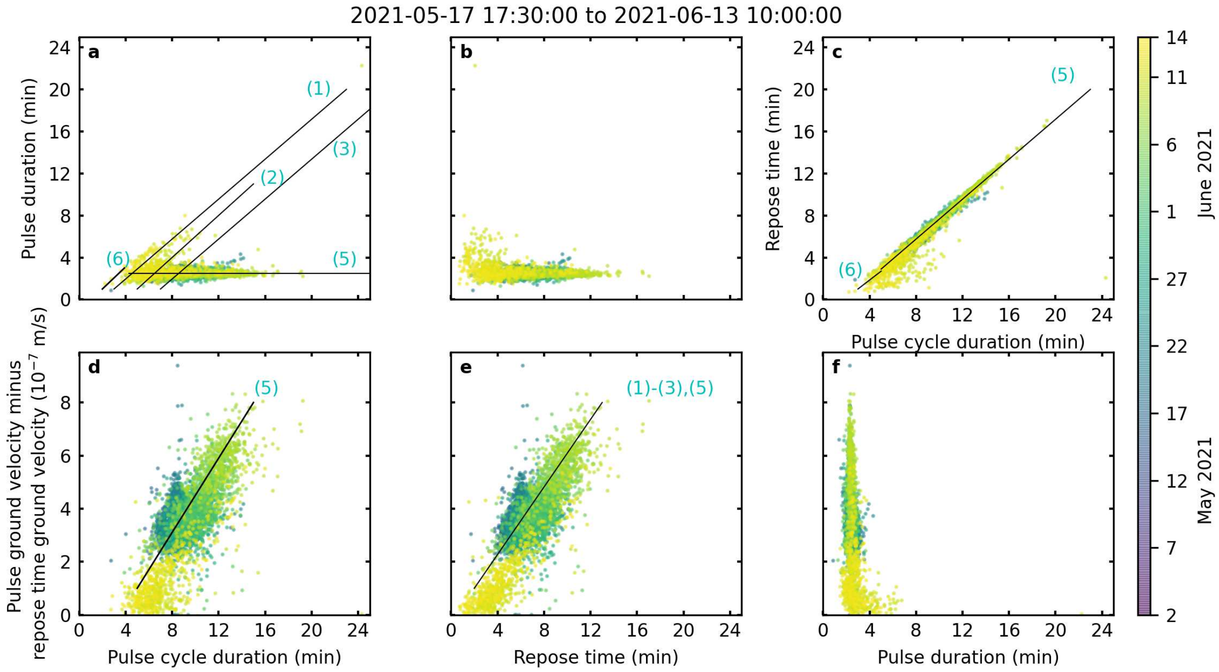

Figure S7: Same as Fig. 5 for points in Period 5.

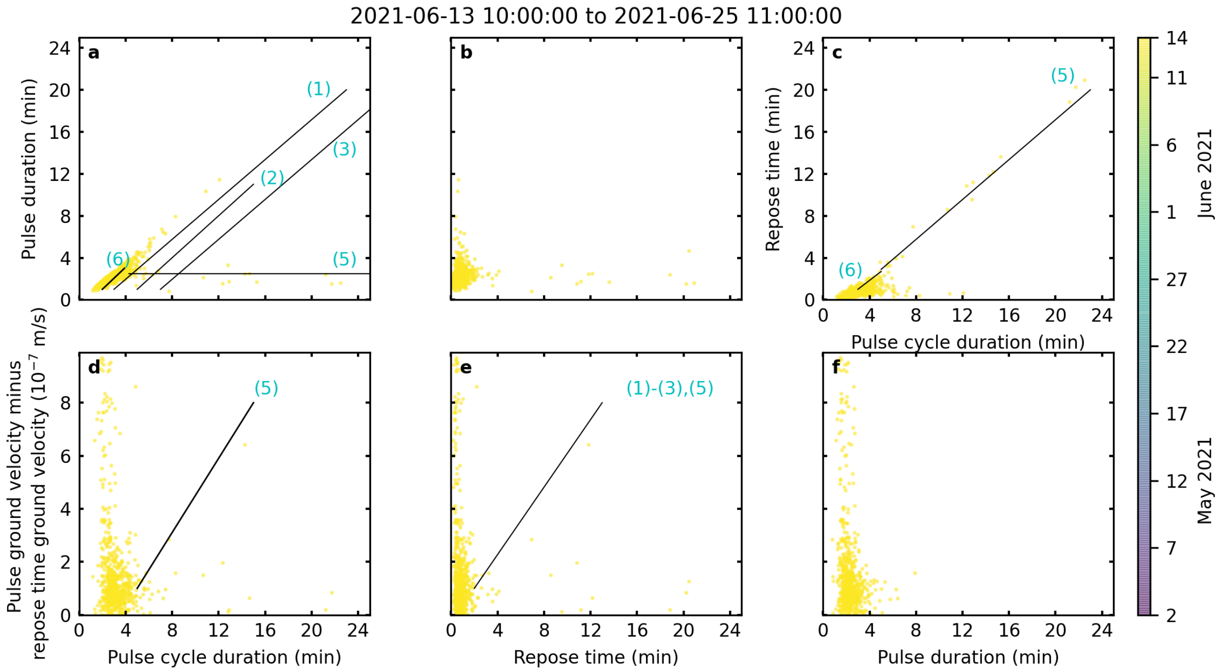

Figure S8: Same as Fig. 5 for points in Period 6.

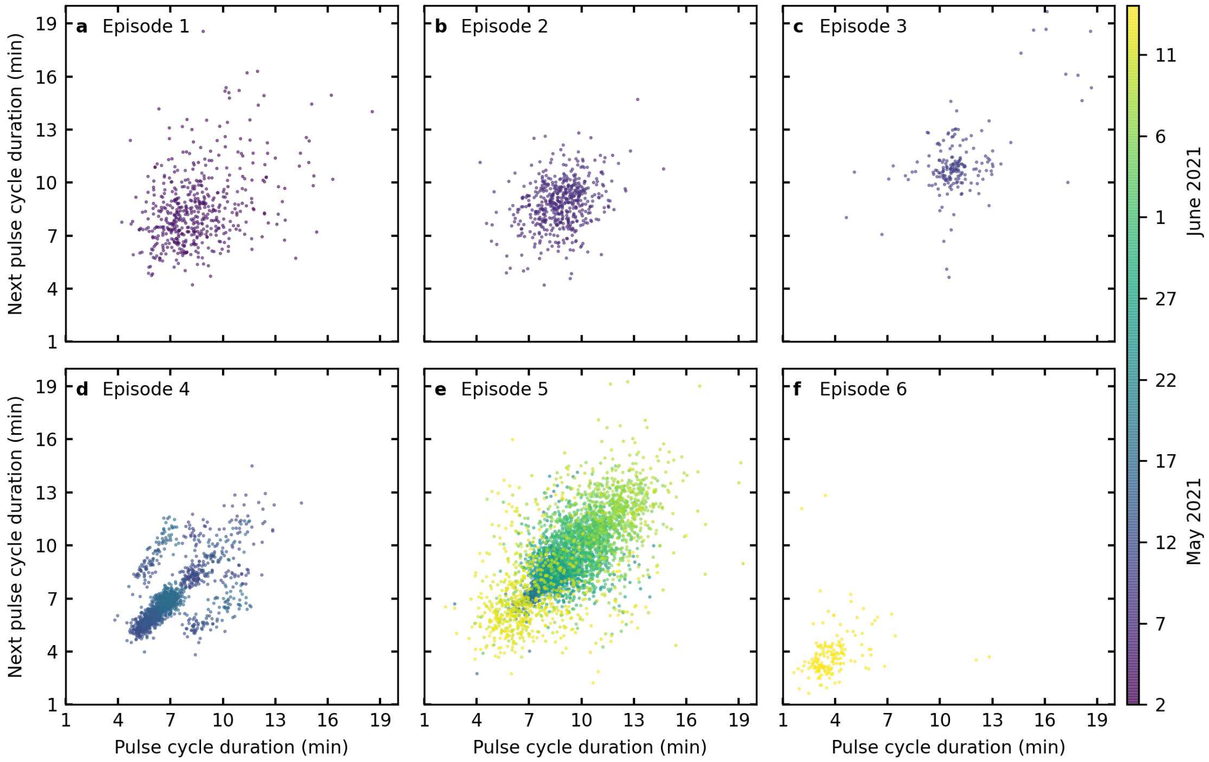

Figure S9: Poincaré plot for pulses in (a) Period 1, (b) Period 2, (c) Period 3, (d) Period 4, (e) Period 5 and (f) Period 6. Subfigure d is further discussed in Fig. 6.